

BAYESIAN TAUT SPLINES FOR ESTIMATING THE NUMBER OF MODES

JOSÉ E. CHACÓN[†] AND JAVIER FERNÁNDEZ SERRANO[‡]

ABSTRACT. The number of modes in a probability density function is representative of the complexity of a model and can also be viewed as the number of subpopulations. Despite its relevance, there has been limited research in this area. A novel approach to estimating the number of modes in the univariate setting is presented, focusing on prediction accuracy and inspired by some overlooked aspects of the problem: the need for structure in the solutions, the subjective and uncertain nature of modes, and the convenience of a holistic view that blends local and global density properties. The technique combines flexible kernel estimators and parsimonious compositional splines in the Bayesian inference paradigm, providing soft solutions and incorporating expert judgment. The procedure includes feature exploration, model selection, and mode testing, illustrated in a sports analytics case study showcasing multiple companion visualisation tools. A thorough simulation study also demonstrates that traditional modality-driven approaches paradoxically struggle to provide accurate results. In this context, the new method emerges as a top-tier alternative, offering innovative solutions for analysts.

1. INTRODUCTION

The concept of *mode* has regained the attention of the research community in recent years (Chacón, 2020). Density modes are defined as local maxima of a probability density function (pdf). As such, they mark regions of relatively high concentration of probability mass. Consequently, they are essential features in *exploratory data analysis*, pointing out new phenomena (Ameijeiras-Alonso et al., 2018; Arias-Castro and Jiang, 2022). Notable application examples include the silica composition of meteors in geology (Good and Gaskins, 1980), the distribution of net income in econometrics (Marron and Schmitz, 1992), and the thickness of stamps in philately (Izenman and Sommer, 1988). Even so, since the true pdf is unknown, estimating it from possibly scarce data is prone to generating *spurious* modes that can be confused with actual discoveries (Good and Gaskins, 1980; Minnotte, 1997).

Concerning modes, two primary considerations emerge: the determination of their quantity and their spatial locations. The latter subsumes the former, but the techniques and hypotheses vary (Chacón, 2020). The number of modes (NoM) is an integer-valued statistical functional, deceptively leading one to believe that *counting* them is more straightforward and less compelling than *locating* them. However, a result by Donoho (1988) states the impossibility of bounding from above this quantity with certain confidence if the underlying finite sample comes from a *genuinely*

[†]DEPARTAMENTO DE MATEMÁTICAS, UNIVERSIDAD DE EXTREMADURA, BADAJOZ, SPAIN.

[‡]DEPARTAMENTO DE MATEMÁTICAS, UNIVERSIDAD AUTÓNOMA DE MADRID, MADRID, SPAIN.

E-mail addresses: [†]jchacon@unex.es ✉, [‡]javier.fernandezs01@estudiante.uam.es.

2020 Mathematics Subject Classification. 62G05 (Primary), 62G07, 62F15, 62C10, 62C86.

Key words and phrases. number of modes, Bayesian inference, compositional spline, kernel density estimation, model selection, mode testing.

[†]<https://orcid.org/0000-0002-3675-1960> .

[‡]<https://orcid.org/0000-0001-5270-9941> .

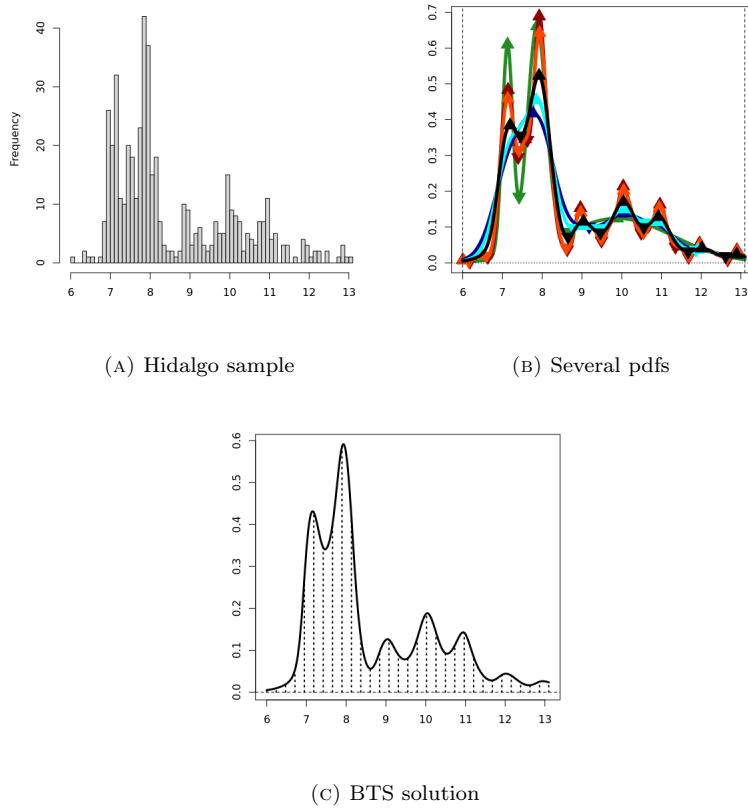


FIG. 1. The Hidalgo stamps data (Izenman and Sommer, 1988). The bar chart on the left displays the sample, which comprises 485 measurements of stamp thickness in hundredths of a millimetre. Several pdfs for that sample are shown on the right. There are some kernel density estimators with different bandwidth selectors, such as PI, LSCV and STE, the first two of which count on variations targeting the r -th pdf derivative (Chacón and Duong, 2013): PI_r and $LSCV_r$. Namely, the pdfs are PI_0 (black, 7 modes), PI_1 (cyan, 5 modes), PI_2 (dark blue, 2 modes), STE (orange, 9 modes), $LSCV_0$ (red, 11 modes), and a Gaussian mixture (green, 3 modes). The bottom picture shows our BTS solution with seven modes based on 32 spline basis functions.

nonparametric distribution. Moreover, from a practical standpoint, the NoM corresponds to the number of groups in many clustering methodologies (Chacón, 2018; Cuevas et al., 2000).

Consider the Hidalgo stamps data, consisting of 485 measurements of stamp thicknesses (Izenman and Sommer, 1988). The raw data histogram is depicted in Fig. 1a. The issue from 1872 comprises a mix of thicknesses deriving from several extinct paper types and manufacturing processes in various factories (Fisher and Marron, 2001). Philatelists are willing to trace the number of sources of that collection to measure the value of the stamp, which calls for estimating the NoM. Interestingly, the problem is open to this day. As Fig. 1b shows, many sensible pdf estimators, such as the *kernel density estimator* (KDE), provide different solutions. Although each new modality approach is traditionally tested on this dataset, no consensus answer exists (Ameijeiras-Alonso et al., 2018). The *Bayesian taut spline* (BTS) method introduced in this paper outputs the pdf in Fig. 1c with seven modes, quantifying the uncertainty of several alternatives.

Goals. This paper addresses the classical problem of estimating the NoM in the univariate setting. We advance the development of new ideas targeting some overlooked themes in modality. Namely, we stress the convenience of structure in the solutions, the uncertain and subjective nature of modes, and the desirability of a holistic view combining global and local properties.

The resulting novel BTS proposal allows incorporating prior knowledge regarding the number and significance of modes while balancing data fitting and model complexity in *soft* solutions, gaining valuable insights along the way. The method will be tested and compared with existing alternatives from the literature in a thorough simulation study based on accuracy.

Highlights.

- Combining kernel estimators and compositional splines benefits mode exploration
- Dimensionality reduction with one principal component captures the essential modes
- Bayesian inference admits expert knowledge regarding modality in soft solutions
- The new proposal and other generic methods outperform classic modality approaches

Related work. Modality research has evolved along several branches. Although BTS is influenced by many of the approaches in this section, its philosophy is reminiscent of the *penalised likelihood* method by Good and Gaskins (1980), which arguably had no straight continuation.

One of the all-time classics is the *critical bandwidth* test by Silverman (1981). The critical bandwidth h_{crit} is the smallest h at which a KDE with a Gaussian kernel has at most k modes. If h_{crit} turns out large after *bootstrapping*, the null hypothesis of k modes is rejected in favour of more than k . Mammen et al. (1992) refined some asymptotic results by Silverman, adjusted the scaling of the bootstrap to increase the power of the test (see also Fisher et al., 1994), and later provided an extension (Fisher and Marron, 2001). Lastly, Hall and York (2001) also suggested a recalibration of the p-values.

An alternative perspective based on the *mass* of the mode was presented by Muller and Sawitzki (1991). Assuming k modes, the *excess mass* $E_k(\lambda)$ is the maximal sum of deviations between the empirical distribution and λ times the Lebesgue measure, where the maximum is taken over all sequences of k disjoint sets (Cheng and Hall, 1998). A large value of $\sup_{\lambda>0} E_k(\lambda) - E_{k-1}(\lambda)$ rejects $k-1$ modes in favour of k . This test statistic for $k=2$ is equivalent in the univariate case to the *dip* test by Hartigan and Hartigan (1985) (see also Cheng and Hall, 1998, 1999; Hall and York, 2001). Polonik (1995a) and Polonik (1995b) further developed the idea of excess mass. Since then, several calibration methods have been proposed (Ameijeiras-Alonso et al., 2018, 2021; Cheng and Hall, 1998, 1999).

Minnotte and Scott (1993) introduced *mode trees*. Using a Gaussian kernel, the sequence of KDEs as h decreases depicts the *branching* of minor modes from larger ones, forming a tree-like diagram. The original version can be extended with visual hints of the location of antimodes and *bumps*, and the mass and significance of each mode (Minnotte, 1997). Minnotte et al. (1998) investigated the use of jittering and bootstrapping techniques to build a *mode forest*, which helps to overcome sampling variability.

Chaudhuri and Marron (1999) developed SiZer, a graphical tool to examine KDEs at different scales. SiZer explores modes attending to statistically significant

sign changes in the first derivative of the KDE at each h . Chaudhuri and Marron (2002) later promoted evaluating second derivatives to complement vanilla SiZer. The multi-scale view was also explored by Dümbgen and Walther (2008). Genovese et al. (2016) introduced a mode testing technique, which estimates the NoM as the maximum number of significant ones at any scale h . Finally, Sommerfeld et al. (2017) used *topological data analysis* to assess modes from a twofold scale-*lifetime* perspective.

Following Hartigan and Hartigan (1985, p. 79), Davies and Kovac (2004) proposed the *taut string*, a piecewise-linear cumulative distribution function (cdf) confined on an ε -radius tube surrounding the empirical cdf (see also Davies et al., 2009). The hyperparameter $\varepsilon > 0$ controls the amount of smoothing, with the NoM monotonically increasing as ε decreases. Interestingly, the taut string minimises the NoM under the ε -radius constraint. A more recent proposal fitting pdfs with a fixed NoM in a dynamical programming scheme is developed in Arias-Castro and Jiang (2022).

Outline. Section 2 provides some technical preliminaries. Then, our novel proposal is presented in Section 3. A real-world sports analytics application is explored in Section 4 for illustrative purposes. The simulation study testing and comparing the performance of the new method to existing alternatives comes in Section 5. Finally, Section 6 discusses the achievements, points of improvement and possibilities of the new method.

2. PRELIMINARIES

The following lines define concepts such as modes, antimodes and modal regions, making our assumptions explicit. We will also introduce the Bayesian inference notation used across all the stages of BTS. Finally, we will recall some elements of KDEs, Bayes spaces and compositional splines necessary for our construction.

In what follows, assume a non-empty and finite dataset $\mathcal{D} = \{x_1, \dots, x_n\} \subset \mathbb{R}$ consisting of n independent and identically distributed (i.i.d.) random variable realisations.

Modes. All intermediate and final univariate pdfs of BTS are assumed to be *Morse functions*, i.e., functions whose critical points are nondegenerate (Chacón, 2015), avoiding pdfs with flat parts where defining modes is more involved (Donoho, 1988, Section 4.1). We will also suppose that all the pdfs f are as smooth as required and have compact support $[a, b]$, i.e., $f(x) > 0$ if $x \in [a, b]$, and $f(x) = 0$ for all $x \notin [a, b]$. Consequently, f will have finitely many critical points (Chacón, 2015, p. 530).

We define *modes* as *local maxima* of the pdf, i.e., points $\hat{m} \in [a, b]$ such that $f(\hat{m}) > f(x)$ for all $x \in [\hat{m} - \epsilon, \hat{m} + \epsilon] \setminus \{\hat{m}\}$, for some $\epsilon > 0$. Such definition includes, but is not limited to, critical points x where $f'(x) = 0$ and $f''(x) < 0$. In particular, the boundaries a and b could be modes despite not obeying the latter derivative constraints (remember that f is defined over \mathbb{R}). Similarly, we define *antimodes* as *local minima* of the pdf, i.e., points $\check{m} \in [a, b]$ such that $f(\check{m}) < f(x)$ for all $x \in [\check{m} - \epsilon, \check{m} + \epsilon] \setminus \{\check{m}\}$, for some $\epsilon > 0$.

Under the previous assumptions, the minimum NoM is one. In general, if there are $k \geq 1$ modes, the number of antimodes will be $k - 1$. For $k > 1$, the modes and antimodes alternate as $a \leq \hat{m}_1 < \check{m}_1 < \hat{m}_2 < \dots < \hat{m}_{k-1} < \check{m}_{k-1} < \hat{m}_k \leq b$. Hence, we see that $[a, b]$ can be expressed as a union of intervals containing exactly one mode: the *modal regions*. More formally, if we write $\hat{m}_0 = a$ and $\hat{m}_k = b$, the i -th modal region containing \hat{m}_i is $[\check{m}_{i-1}, \hat{m}_i]$, where \hat{m}_i is allowed to coincide with

one of the boundaries only if $i = 1$ or $i = k$. With that notation, when $k = 1$, the unique modal region is $[\hat{m}_0, \hat{m}_1] = [a, b]$.

Bayesian inference. Continuous and discrete parameters and hypotheses are treated as random variables in Bayesian inference. We will use the same notation $\Pr(\cdot)$ for pdfs and probability mass functions, inferring the continuous/discrete nature from the context.

Consider a parameter vector $\boldsymbol{\theta} = (\theta_1, \dots, \theta_m) \in \mathbb{R}^m$. We will refer to its Bayesian prior as $\Pr(\theta_1, \dots, \theta_m)$. The model pdf conditioning on $\boldsymbol{\theta}$ will be denoted as $\Pr(\cdot|\theta_1, \dots, \theta_m)$. Then, $\Pr(\mathcal{D}|\theta_1, \dots, \theta_m) = \prod_{x \in \mathcal{D}} \Pr(x|\theta_1, \dots, \theta_m)$ is the likelihood of $\boldsymbol{\theta}$ given data \mathcal{D} , and $\Pr(\theta_1, \dots, \theta_m|\mathcal{D}) \propto \Pr(\mathcal{D}|\theta_1, \dots, \theta_m) \times \Pr(\theta_1, \dots, \theta_m)$ is the posterior of $\boldsymbol{\theta}$ given \mathcal{D} , where “ \propto ” indicates proportionality, i.e., equality except for a normalising constant making the left-hand side a pdf or a probability mass function. To specify a value $\vartheta \in \mathbb{R}$ for some parameter θ_i , we will replace the parameter “ θ_i ” with “ $\theta_i = \vartheta$ ” in the notations above.

Kernel density estimation. The KDE for the dataset \mathcal{D} based on a Gaussian kernel ϕ and bandwidth $h > 0$ is the function $\mathbb{R} \rightarrow (0, \infty)$ defined by

$$\hat{f}_h(x) = \frac{1}{nh} \sum_{i=1}^n \phi\left(\frac{x - x_i}{h}\right). \quad (1)$$

The parameter h controls the amount of smoothing. Fixing \mathcal{D} , a large value of h hides prominent features, while a small one produces spurious *wiggles*. A Gaussian kernel is needed to ensure continuous tracking of modes (Minnotte and Scott, 1993; Silverman, 1981).

Bayes spaces. The *Bayes space* $\mathcal{B}[a, b]$ of positive pdfs with bounded support $[a, b]$ and square-integrable logarithm has a Hilbert space structure (Machalová et al., 2020) originating from mapping $f \in \mathcal{B}[a, b]$ to the household $L^2([a, b])$ via the *centred log-ratio* (CLR) transformation

$$\text{clr}[f](x) = \log f(x) - \frac{1}{b-a} \int_a^b \log f(y) dy. \quad (2)$$

Since $\int_a^b \text{clr}[f](x) dx = 0$, if we consider the subset complying with that zero-integral constraint, $L_0^2([a, b]) = \{p \in L^2([a, b]) : \int_a^b p(x) dx = 0\}$, then $\mathcal{B}[a, b]$ is isometric to $L_0^2([a, b])$ with inverse $\text{clr}^{-1}[p](x) = \exp p(x) / \int_a^b \exp p(y) dy$. The vector space operations of sum (perturbation) and scalar multiplication (powering) are, respectively, $(f \oplus g)(x) = f(x)g(x) / \int_a^b f(y)g(y)dy$, and $(\gamma \odot f)(x) = f(x)^\gamma / \int_a^b f(y)^\gamma dy$, where $f, g \in \mathcal{B}[a, b]$ and $\gamma \in \mathbb{R}$. Let us denote $f \ominus g = f \oplus (-1) \odot g$. Similarly, the inner product between $f, g \in \mathcal{B}[a, b]$ is given by

$$\langle f, g \rangle_{\mathcal{B}} = \frac{1}{2(b-a)} \int_a^b \int_a^b \log \frac{f(x)}{f(y)} \log \frac{g(x)}{g(y)} dx dy, \quad (3)$$

that is, $\langle f, g \rangle_{\mathcal{B}} = \int_a^b \text{clr}[f](x) \text{clr}[g](x) dx = \langle \text{clr}[f], \text{clr}[g] \rangle_2$.

Compositional splines. Let us fix a polynomial degree $r \geq 3$, enabling a non-flat second derivative. Given $d \geq r$, we can construct a d -dimensional vector subspace $\mathcal{Z}_d[a, b] \subset \mathcal{B}[a, b]$ consisting of pdfs whose CLR transformations (2) are r -th degree spline functions $s : [a, b] \rightarrow \mathbb{R}$ such that $\int_a^b s(x) dx = 0$. The elements in $\mathcal{Z}_d[a, b]$ are known as *compositional splines*.

Explicitly constructing compositional splines relies on a variant of the usual B-splines, known as ZB-splines, obeying the zero-integral constraint (Machalová et al., 2020). Let us split $[a, b]$ through arbitrary knots $a = \kappa_0 < \dots < \kappa_{d-r+1} = b$. Then,

we can define d ZB-spline basis functions $Z_1, \dots, Z_d : [a, b] \rightarrow \mathbb{R}$ built up from r -th degree polynomials joining at the knots with maximal $C^{r-1}([a, b])$ smoothness.

Let us define the ZB-spline $z_\theta = \sum_{i=1}^d \theta_i Z_i$, for $\theta = (\theta_1, \dots, \theta_d) \in \mathbb{R}^d$. The CLR back-transformed pdf $\zeta_\theta = \text{clr}^{-1}[z_\theta] = \bigoplus_{i=1}^d (\theta_i \odot \text{clr}^{-1}[Z_i])$ is a compositional spline. Therefore, we can define $\mathcal{Z}_d[a, b] = \{\zeta_\theta : \theta \in \mathbb{R}^d\}$. Note that $\mathcal{Z}_d[a, b]$ is isometric to \mathbb{R}^d via $\zeta_\theta \mapsto \theta$ with inner product $\langle \zeta_{\theta_1}, \zeta_{\theta_2} \rangle_{\mathcal{B}} = \theta_1^\top \mathbf{M} \theta_2$, for $\theta_1, \theta_2 \in \mathbb{R}^d$, where the symmetric matrix \mathbf{M} has entries $\mathbf{M}_{ij} = \langle Z_i, Z_j \rangle_2$.

Every $f \in \mathcal{B}[a, b]$ can be approximated in the least squares sense within $\mathcal{Z}_d[a, b]$ provided equidistant knots and a sufficiently large d are used. The value r is less critical, making $r = 3$ a widespread choice. Let us fix a fine grid with evenly spaced points $a = t_1 < \dots < t_m = b$. For all $f \in \mathcal{B}[a, b]$ and every smoothing penalty factor $\alpha \in (0, 1)$, we define the curvature-penalised quadratic loss of a parameter vector $\theta \in \mathbb{R}^d$ as

$$\mathcal{L}(\theta; f, \alpha) = \alpha \sum_{i=1}^m \{\text{clr}[f](t_i) - z_\theta(t_i)\}^2 + (1 - \alpha) \int_a^b z_\theta''(x)^2 dx. \quad (4)$$

The sum term relates to data fitting, whereas the integral value amounts to the *total curvature* of the spline, representing its complexity. Then, the compositional spline $[f]_\alpha$ approximating $f \in \mathcal{B}[a, b]$ with smoothing penalty factor $\alpha \in (0, 1)$ is

$$[f]_\alpha = \zeta_{\hat{\theta}(f, \alpha)}, \quad \text{where } \hat{\theta}(f, \alpha) = \arg \min_{\theta \in \mathbb{R}^d} \mathcal{L}(\theta; f, \alpha). \quad (5)$$

Problem (5) has a straightforward linear algebra solution (Machalová et al., 2020). The larger α , the closer (5) is to f . In contrast, smaller values of α produce smoother solutions. If f is positive but does not have bounded support $[a, b]$, we will assume that $[f]_\alpha \equiv [f^*]_\alpha$, where the pdf f^* satisfies $f^*(x) \propto f(x) \cdot \mathbb{1}_{[a, b]}(x)$, since $\text{clr}[f]$ and $\text{clr}[f^*]$ coincide over $[a, b]$.

3. THE BAYESIAN TAUT SPLINE (BTS) METHOD

This section introduces the new BTS method, encompassing several steps. First, an *exploration* phase scans the KDE mode tree while building spline models. Next, an *analysis* phase summarises the splines into a linear one-parameter model. Then, a *selection* phase obtains probabilities and pdfs for each k -mode hypothesis. Finally, a *testing* phase evaluates the modes of each representative k -modal pdf.

We refer the reader to the supplementary material (SM) (Chacón and Fernández Serrano, 2023) for implementation details and discussing the pillars of the proposal: model structure, Bayesian inference and a holistic view joining global and local density properties.

We will illustrate the different stages through the example in Fig. 2. Fig. 2a depicts a complicated case with three modes, where two are little pronounced. The NoM in the resulting random sample in Fig. 2b is debatable, for one of the two apparent modes on the left block seems isolated and weak. We shall see how BTS handles the situation.

3.1. Exploration. BTS starts off exploring modes through a combination of KDEs and compositional splines. Informally speaking, for every KDE bandwidth $h > 0$ and smoothing penalty factor $\alpha \in (0, 1)$, we first build the KDE \hat{f}_h from \mathcal{D} and then fit a compositional spline to \hat{f}_h using least squares with penalty α . More formally, for every pair of smoothing parameters $(h, \alpha) \in (0, \infty) \times (0, 1)$, we define a pdf model for \mathcal{D} conditioning on an uncertain pair (h, α) as

$$\Pr(\cdot | h, \alpha) = [\hat{f}_h]_\alpha. \quad (6)$$

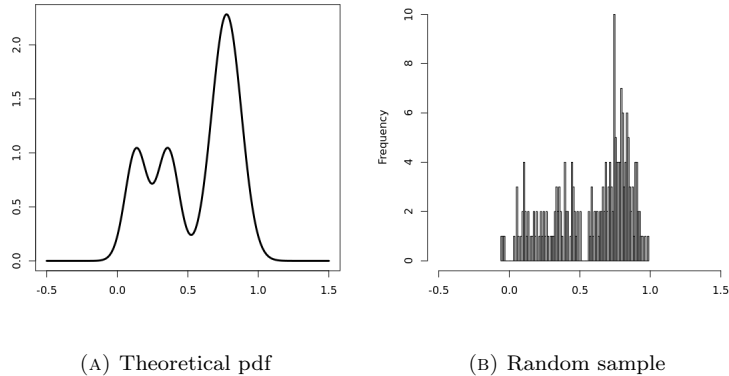


FIG. 2. An illustrative test-bed for estimating the NoM. The M25 mixture model pdf from Ameijeiras-Alonso et al. (2018) is shown on the left. A histogram of a random sample of size 200 from that model is displayed on the right.

Since \hat{f}_h in (6) has unbounded support, we will set $a = \min(\mathcal{D})$ and $b = \max(\mathcal{D})$ in practice. In this context, let us abbreviate for later use $\hat{\boldsymbol{\theta}}(h, \alpha) \equiv \hat{\boldsymbol{\theta}}(\hat{f}_h, \alpha)$, where the right-hand side is as in (5).

The KDE is known to be sensitive to outliers in the tails (Chacón and Duong, 2013). Spurious modes, almost invisible to the human eye, might appear despite the curvature penalisation of BTS in cases with severely isolated points. We propose removing the outliers before building the KDE in (6), similarly to Chacón and Duong (2013, Section 5.2). Using (1) as a pilot, one can calculate the probability masses of all the modal regions and remove those $x \in \mathcal{D}$ linked to underrepresented modes. After removal, the resulting subsample is again fed to (1). This preprocessing step shall be implicitly assumed in (6) in the upcoming sections.

Model (6) is not a typical parametric pdf, for (h, α) are a *proxy* of the underlying spline coordinates $\boldsymbol{\theta}$. Since direct likelihood-based estimation tends to *overfit* data, especially with discretised data, we suggest imposing strong regularity conditions through a prior $\Pr(h, \alpha)$. Then, exploring the spline space and the subsequent modes comes down to evaluating the posterior $\Pr(h, \alpha | \mathcal{D})$. This can be achieved via Markov chain Monte Carlo (MCMC) simulation (Kass and Raftery, 1995), securing a posterior sample $\mathcal{S} = \{(h_i, \alpha_i)\}_{i=1}^{\nu}$.

We propose an *improper* prior $\Pr(h, \alpha) \equiv \Pr(h) \times \Pr(\alpha) \times \Pr(k) \times \Pr(\xi)$ factoring the shape parameters alongside quantities representing the complexity of the true pdf, such as $k \equiv k(h, \alpha)$, the NoM of $\Pr(\cdot | h, \alpha)$, and $\xi \equiv \xi(h, \alpha)$, the total curvature term in (4) with $\boldsymbol{\theta} = \hat{\boldsymbol{\theta}}(h, \alpha)$. See Good and Gaskins (1980, p. 45) for a similar use of an “improper” prior in regularisation. A design with well-known parametric distributions is

$$\begin{aligned}
 h &\sim \text{LogNormal}(\mu = \mu_h, \sigma = \sigma_h), \\
 1 - \alpha &\sim \text{Beta}(\alpha = 1, \beta = \beta_{1-\alpha}), \\
 k &\sim \text{Poisson}(\lambda = 1), \\
 \xi &\sim \text{Exponential}(\lambda = \lambda_\xi).
 \end{aligned} \tag{7}$$

See the SM (Chacón and Fernández Serrano, 2023) for justification of the previous scheme and the selection of μ_h , σ_h , $\beta_{1-\alpha}$ and λ_ξ , depending on the case.

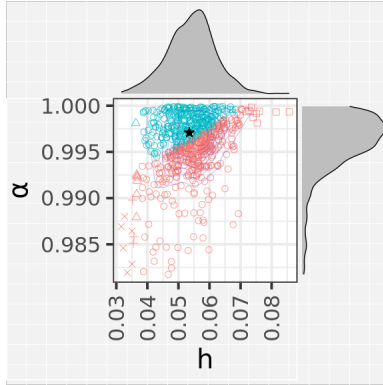


FIG. 3. MCMC sample from $\Pr(h, \alpha | \mathcal{D})$ consisting of 700 observations. The horizontal and vertical axes represent the h and α components, respectively. The points are coloured according to the NoM of model (6): red (57% of the total, 2 modes) and blue (43% of the total, 3 modes). The shape of each point represents the NoM of the underlying KDE, thus only depending on h : square (2 modes), circle (3 modes) and triangle (4 modes), among others. The average point is the black star in the middle of the point cloud. KDEs for the margins are also provided.

The first BTS estimator for the NoM shall be called the *raw* variant of BTS. It is the most frequent modality in \mathcal{S} , i.e.,

$$\hat{k}_{\text{BTS},0} = \arg \max_{k \in \mathbb{N}} |\{i \in \{1, \dots, \nu\} : \Pr(\cdot | h = h_i, \alpha = \alpha_i) \text{ has } k \text{ modes}\}|, \quad (8)$$

where the lower k should be taken for parsimony in case of a draw. The same criterion shall also apply to the upcoming estimators. The counts in (8) can also be normalised to obtain probabilities for each k hypothesis, gaining more insight. We will further process \mathcal{S} in the analysis phase.

Fig. 3 shows the results from the exploration phase of BTS on the random sample in Fig. 2b. The two main scenarios, of two and three modes, are considered in the MCMC sample. The former hypothesis has an inconclusive advantage with 57% of the *ballots*. Because of the intended conservatism of this stage, BTS sticks to two modes without overlooking three. Fig. 3 displays some compelling features of BTS. The spline structure and regularisation leave a fourth and a fifth mode in the underlying KDE with no effect, restraining excessive complexity. Similarly, many points correspond to partially *ironed* three-mode KDEs. We can graphically see a neat oblique line separating the two modality hypotheses, meaning KDEs and smoothing splines benefit from each other to test modes.

Revisiting the classic Hidalgo example in Fig. 1, the above prior design oriented to discrete data leads in (8) to $\hat{k}_{\text{BTS},0} = 7$ with 100% probability. This unanimity ensures that this seven-mode result stands through the upcoming stages.

3.2. Analysis. The exploration phase of BTS could benefit from some improvement. Since $\Pr(h, \alpha | \mathcal{D})$ is not genuinely parametric, we depend on finite bivariate MCMC samples. Robust approximations require long MCMC chains, and solving (6) at each iteration is time-consuming. On the other hand, although $\Pr(h, \alpha | \mathcal{D})$ captures modes thoroughly, mode trees count on just one parameter, h , making them easier to interpret (Minnotte and Scott, 1993). The analysis stage of BTS will address both issues.

Analysing \mathcal{S} is problematic, for (h, α) does not reflect the spline structure. Instead, let us define $\theta_i = \hat{\theta}(h_i, \alpha_i)$ for every $(h_i, \alpha_i) \in \mathcal{S}$. We propose a dimensionality reduction on the pdf sample $\{\zeta_{\theta_i}\}_{i=1}^{\nu} \subset \mathcal{Z}_d[a, b]$ using *simplicial functional*

principal component analysis (SFPCA) (Hron et al., 2016). SFPCA works similarly to its non-functional counterpart, expressing the compositional spline space in terms of orthonormal axes $\text{PC}_1, \dots, \text{PC}_d \in \mathcal{Z}_d[a, b]$ (each one, a principal component (PC)) with respective variances $\lambda_1 \geq \dots \geq \lambda_d$. Then, the usual next step is to simplify a sample by projecting each centred functional datum over a few PCs that retain a considerable proportion of the original variability. See the SM (Chacón and Fernández Serrano, 2023) for a brief note on SFPCA in our context.

Beyond convenience and simplicity, a single PC provides enough power in the BTS context. See the SM (Chacón and Fernández Serrano, 2023) for justification. We propose a refined pdf model for \mathcal{D} depending on a single parameter δ through

$$\Pr(\cdot|\delta) = \mu \oplus \delta \odot \sigma, \quad (9)$$

where $\mu = (1/\nu) \odot \bigoplus_{i=1}^{\nu} \zeta_{\theta_i}$ is a sample average pdf, and $\sigma = \sqrt{\lambda_1} \odot \text{PC}_1$ is a standard deviation pdf along the first PC. Even though δ could range over the whole \mathbb{R} , extrapolation beyond certain limits leads to nonsensical solutions. We can assess sensible values for δ by inspecting the centred projections along PC_1 , i.e., the scores $s_i = \langle \zeta_{\theta_i} \ominus \mu, \text{PC}_1 \rangle_{\mathcal{B}}$. If we write $\delta_i = s_i/\sqrt{\lambda_1}$, we can build a *support* for δ as $\Delta = [\delta_{\min}, \delta_{\max}]$, where $\delta_{\min} = \min_{1 \leq i \leq \nu} \delta_i$ and $\delta_{\max} = \max_{1 \leq i \leq \nu} \delta_i$. Provided $\delta \in \Delta$, (9) represents the modal features in $\Pr(h, \alpha|\mathcal{D})$.

Since (9) captures the essential parts of (6) by construction, one can adopt a more *objective* approach for the prior distribution. The Jeffreys prior is a standard alternative in a univariate setting (Bernardo, 1994). It assigns equal probabilities to regions of the statistical manifold (9) with the same *volume*, conveying the *principle of indifference*. Additionally, the Jeffreys prior is invariant to reparametrisation. Also, note that since Δ is bounded, the Jeffreys prior is *proper*, integrating up to one. Finally, straightforward calculations for this type of prior yield, for $\delta \in \Delta$,

$$\Pr(\delta) \propto \sqrt{\text{Var}(\log \sigma(X_{\delta}))}, \text{ where } X_{\delta} \sim \Pr(\cdot|\delta), \quad (10)$$

and $\text{Var}(\cdot)$ denotes the variance of a random variable. We can see that $\Pr(\delta) > 0$ for all $\delta \in \Delta$, since σ can never be constant and $\Pr(x|\delta) > 0$ for all $x \in [a, b]$.

We will refer to the combination of (9) and (10) as the SFPCA model of BTS. BTS considers a second Bayesian inference on the SFPCA model to estimate the NoM.

Fig. 4 shows the results of the analysis stage after the exploration in Fig. 3. First, Fig. 4a plots the PCs against their variances. The sudden drop is characteristic, justifying keeping one dimension. Then, Fig. 4b sheds some light on the shape of the splines in the sample in Fig. 3. All the uncertainty gravitates around whether the left block splits into two modes. The mean μ has three modes, one of which is barely noticeable as an incipient *shoulder* that finally emerges as the left-most mode of $\mu \oplus \delta_{\max} \odot \sigma$.

3.3. Selection. The SFPCA model encompasses several hypotheses about the NoM of the pdf. Indeed, the prior (10) is an *encompassing prior* (Klugkist et al., 2005), expressing the relative uncertainty of δ under different domain restrictions. More precisely, let us define, for $k \in \mathbb{N}$, $\Delta_k = \{\delta \in \Delta : \Pr(\cdot|\delta) \text{ has } k \text{ modes}\}$, i.e., the set of parameters δ producing k modes, and let $\mathcal{K} = \{k \in \mathbb{N} : \Delta_k \neq \emptyset\}$ be the set of all the reachable modality numbers. For every $k \in \mathcal{K}$, we can define a prior ensuring k modes as

$$\Pr(\delta|k) \propto \Pr(\delta) \cdot \mathbb{1}_{\Delta_k}(\delta). \quad (11)$$

Combining the new priors (11) with the original model (9), we obtain a class of SFPCA k -modal pdfs. This way, BTS translates estimating the NoM into a Bayesian model selection problem.

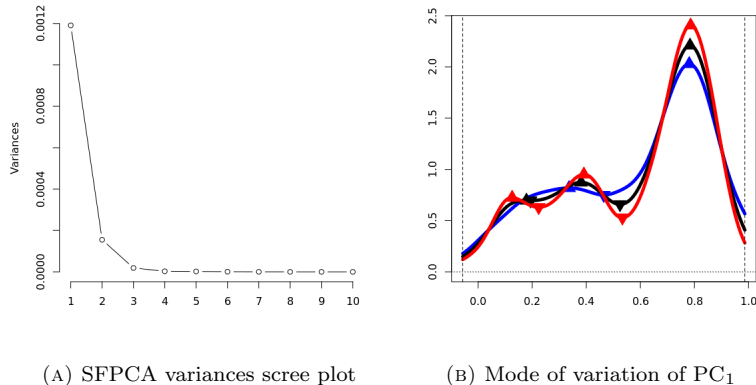


FIG. 4. SFPCA analysis phase results. The scree plot of the ordered PCs against their variances is presented on the left. Some representative pdfs in the SFPCA model (9) are displayed on the right: the mean μ (black, 3 modes), the lower bound $\mu \oplus \delta_{\min} \odot \sigma$ (blue, 2 modes) and the upper bound $\mu \oplus \delta_{\max} \odot \sigma$ (red, 3 modes).

Note that \mathcal{K} is finite since the pdfs (9) are derived from splines. From our experience, we can virtually assure that every $k \in \mathcal{K}$ shows up as the modality of some pdf in the exploratory sample \mathcal{S} . However, it is not uncommon for some modalities observed in the exploration phase to be absent in \mathcal{K} . This loss of information, which is welcomed for parsimony, roots in dimensionality reduction.

The *marginal likelihood* of the k -modal prior, $k \in \mathcal{K}$, and the total prior, respectively, are $\Pr(\mathcal{D}|k) = \int_{\Delta} \Pr(\mathcal{D}|\delta) \times \Pr(\delta|k) d\delta$ and $\Pr(\mathcal{D}) = \int_{\Delta} \Pr(\mathcal{D}|\delta) \times \Pr(\delta) d\delta$. After assigning prior probabilities $\Pr(k)$ to each hypothesis $k \in \mathbb{N}$, we can calculate the posterior probabilities (Wasserman, 2000) as $\Pr(k|\mathcal{D}) \propto \Pr(\mathcal{D}|k) \times \Pr(k)$, assuming that $\Pr(k|\mathcal{D}) = 0$ whenever $k \notin \mathcal{K}$.

Calculating $\Pr(\mathcal{D}|k)$ is generally intractable (Kass and Raftery, 1995). Instead, we can use the fact that, in the case of an encompassing prior (Klugkist et al., 2005, p. 60), for every $k \in \mathcal{K}$, we have $\Pr(\mathcal{D}|k)/\Pr(\mathcal{D}) = \int_{\Delta_k} \Pr(\delta|\mathcal{D}) d\delta / \int_{\Delta_k} \Pr(\delta) d\delta$, where the denominator on the right-hand side is positive. This ratio of marginal likelihoods is the *Bayes factor*. Plugging it into the equation for $\Pr(k|\mathcal{D})$ above, we get

$$\Pr(k|\mathcal{D}) \propto \frac{\int_{\Delta_k} \Pr(\delta|\mathcal{D}) d\delta}{\int_{\Delta_k} \Pr(\delta) d\delta} \times \Pr(k). \quad (12)$$

Based on (12), a sensible choice for the prior is $\Pr(k) = \int_{\Delta_k} \Pr(\delta) d\delta$. However, $\Pr(k) \propto 1$ is usually preferred (Kass and Raftery, 1995; Klugkist et al., 2005). Furthermore, we can consider the prior probabilities from the posterior sample \mathcal{S} in the exploration phase.

Maximising the posterior probability (12), we finally get the *processed* estimator variant of BTS:

$$\hat{k}_{\text{BTS},1} = \arg \max_{k \in \mathbb{N}} \Pr(k|\mathcal{D}). \quad (13)$$

In addition to the new insights gained through the process, the latter estimator will generally produce better results than (8), as demonstrated later in Section 5. The testing phase of BTS, introduced in Section 3.4 below, will further refine (13), providing yet more information.

One can easily verify that, for all $k \in \mathcal{K}$, the Bayesian update to the k -modality prior (11) is $\Pr(\delta|k, \mathcal{D}) \propto \Pr(\delta|\mathcal{D}) \cdot \mathbb{1}_{\Delta_k}(\delta)$. Hence, the prior $\Pr(\delta|\mathcal{D})$ in (12) can

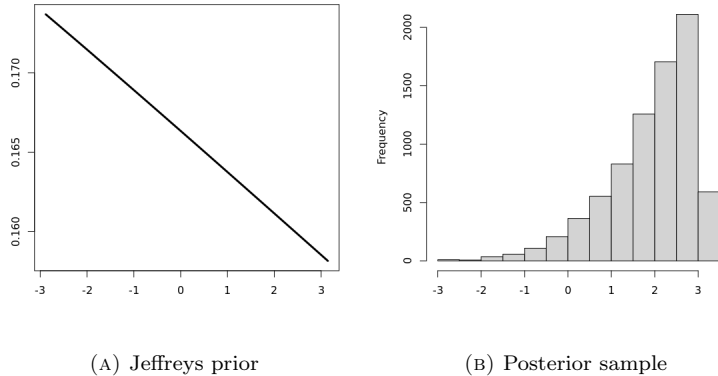


FIG. 5. Second Bayesian inference on the SFPCA model. The Jeffreys prior pdf (10) is shown on the left. A histogram of a sample from $\Pr(\delta|\mathcal{D})$ consisting of 7,840 observations is shown on the right.

be used to obtain a representative pdf of the k -modality hypothesis, typically summarising $\Pr(\delta|k, \mathcal{D})$ (Bernardo, 1994). However, neither the *posterior predictive distribution* nor the *posterior mean* preserves the NoM. A common choice in such circumstances is the *posterior median*, which belongs to Δ_k . The median Bayes estimator can then be interpreted as the minimiser of the average distance induced by (3).

Fig. 5 shows the before and after of the second inference. Fig. 5a depicts the Jeffreys prior (10), which exhibits a slight slope, mildly penalising the more complex pdfs. Then, Fig. 5b shows a histogram of the posterior sample displaying a varying slope in the opposite direction. The Bayesian update for the SFPCA model favours the three-mode hypothesis more than the exploratory inference, as confirmed by Fig. 6. Regardless of the choice of $\Pr(k)$ (among those proposed here), BTS correctly selects three modes based on posterior probabilities ranging between 0.92 and 0.94.

3.4. Testing. The NoM in BTS measured *model complexity* in Section 3.1 and was a *feature* encompassing a range of parameter values in Section 3.3. Both correspond to *global* views. However, modes are defined locally, which calls for testing their significance with nearby data. We thus invoke the concept of *excess mass region*.

For every $k \in \mathcal{K}$ modality hypothesis, let us call \tilde{f}_k the median k -modal pdf selected in Section 3.3 with probability $\Pr(k|\mathcal{D})$. Then, for the i -th mode \hat{m}_i of the model \tilde{f}_k , we define the i -th excess mass region as $\mathcal{M}_{k,i} = \{x \in [\tilde{m}_{i-1}, \tilde{m}_i] : \tilde{f}_k(x) \geq \eta_i\}$, where \tilde{m}_{i-1} and \tilde{m}_i are the minimum and the maximum, respectively, of the modal region corresponding to \hat{m}_i , and $\eta_i = \max\{\tilde{f}_k(x) : x \in \{\tilde{m}_{i-1}, \tilde{m}_i\} \setminus \{\hat{m}_i\}\}$. Naturally, $\hat{m}_i \in \mathcal{M}_{k,i}$. These excess mass regions are a slight variation of those considered in Minnotte and Scott (1993) to allow modes to appear at modal region boundaries.

The rationale behind excess mass regions is as follows. Let $d(f_1, f_2)$ denote the distance between two functions $f_1, f_2 \in L^1([a, b])$. Then, define, for $x \in [a, b]$,

$$g_{k,i}(x) = \begin{cases} \eta_i, & \text{if } x \in \mathcal{M}_{k,i} \\ \tilde{f}_k(x), & \text{if } x \in [a, b] \setminus \mathcal{M}_{k,i} \end{cases}.$$

As mentioned in Minnotte and Scott (1993), for any continuous f without local maxima in $[\tilde{m}_{i-1}, \tilde{m}_i]$, we have $d(\tilde{f}_k, g_{k,i}) \leq d(\tilde{f}_k, f)$. In other words, $g_{k,i}$ is the

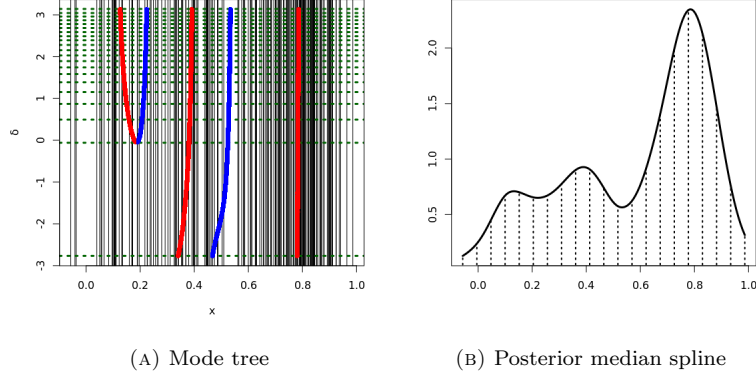


FIG. 6. Results of the BTS method. The left-hand side picture shows a mode tree with δ values on the vertical axis. Red points correspond to modes, whereas the blue ones are antimodes. The black vertical lines highlight the original sample observations in Fig. 2b. The dashed green horizontal lines represent uniform quantiles of the posterior sample in Fig. 5b. The figure on the right displays the posterior median model, which has three modes and a CLR dimension of 22.

least distinguishable function from \tilde{f}_k with such constraints. This suggests that, to test the existence of \hat{m}_i , assuming \tilde{f}_k is true, the most conservative null hypothesis of non-existence should be based on $g_{k,i}$. Since $g_{k,i}$ only differs from \tilde{f}_k in being constant over $\mathcal{M}_{k,i}$, we see an identification between removing \hat{m}_i and being *uniform* over $\mathcal{M}_{k,i}$.

Given a k -modality hypothesis, we can *zoom in* on the i -th excess mass region to test the strength of evidence in favour of \hat{m}_i locally. Let us define a one-parameter power variation of \tilde{f}_k around $\mathcal{M}_{k,i}$ through

$$\Pr(x|\tau, k, i) \propto (\tau \odot \tilde{f}_k)(x) \cdot \mathbb{1}_{\mathcal{M}_{k,i}}(x), \quad (14)$$

where $\tau \in [0, \infty)$. We note that (14) coincides with the τ -powering of the restriction of \tilde{f}_k to $\mathcal{M}_{k,i}$, which is retrieved for $\tau = 1$. Powering has the effect of intensifying or weakening the mode at \hat{m}_i . For a large τ , the probability mass concentrates around \hat{m}_i , while for a small τ , the mass is spread over $\mathcal{M}_{k,i}$, reaching uniformity for $\tau = 0$. This observation motivates a mode significance test in which the null hypothesis \mathcal{H}_0 of the non-existence of the mode is paired with $\tau = 0$, while $\tau \neq 0$ represents the alternative hypothesis \mathcal{H}_1 of existence. This way, testing the mode becomes a Bayesian single-parameter value testing problem.

The Savage-Dickey method (Wagenmakers et al., 2010) assigns probabilities to \mathcal{H}_0 and \mathcal{H}_1 , weighing the evidence in data \mathcal{D} with prior knowledge. Namely, we can transform prior odds into posterior odds via

$$\frac{\Pr(\mathcal{H}_1|\mathcal{D}, k, i)}{\Pr(\mathcal{H}_0|\mathcal{D}, k, i)} = \frac{\Pr(\mathcal{D}|\mathcal{H}_1, k, i)}{\Pr(\mathcal{D}|\mathcal{H}_0, k, i)} \times \frac{\Pr(\mathcal{H}_1|k, i)}{\Pr(\mathcal{H}_0|k, i)}. \quad (15)$$

We will denote the prior odds for \mathcal{H}_1 as $\text{Odds}(\mathcal{H}_1|k, i) = \Pr(\mathcal{H}_1|k, i)/\Pr(\mathcal{H}_0|k, i)$, and those in favour of \mathcal{H}_0 as $\text{Odds}(\mathcal{H}_0|k, i) = \text{Odds}(\mathcal{H}_1|k, i)^{-1}$. If $\text{Odds}(\mathcal{H}_1|k, i) = 0$, we shall assume $\Pr(\mathcal{H}_1|\mathcal{D}, k, i) = 0$. At this point, one usually takes $\Pr(\mathcal{H}_0|k, i) = \Pr(\mathcal{H}_1|k, i)$, making the posterior odds equal a ratio of marginal likelihoods, the *Bayes factor*, where

$$\Pr(\mathcal{D}|\mathcal{H}_1, k, i) = \int_0^\infty \Pr(\mathcal{D}|\tau, k, i) \times \Pr(\tau|k, i) d\tau, \quad (16)$$

and $\Pr(\mathcal{D}|\mathcal{H}_0, k, i) = \Pr(\mathcal{D}|\tau = 0, k, i)$. The likelihood $\Pr(\mathcal{D}|\tau, k, i)$ is evaluated only with data in the excess mass region, i.e., $\Pr(\mathcal{D}|\tau, k, i) = \prod_{x \in \mathcal{D} \cap \mathcal{M}_{k,i}} \Pr(x|\tau, k, i)$. Whenever $\mathcal{D} \cap \mathcal{M}_{k,i} = \emptyset$, we can assume $\Pr(\mathcal{H}_1|\mathcal{D}, k, i) = 0$. A natural prior density choice is $\tau|k, i \sim \text{Exponential}(\lambda = 1)$, regardless of k and i . Hence, τ has mean one and a global mode at zero, favouring the null hypothesis and leaning the average scenario towards \tilde{f}_k .

Computing (16) is generally complicated (Kass and Raftery, 1995). However, defining the posterior $\Pr(\tau|\mathcal{D}, k, i) \propto \Pr(\mathcal{D}|\tau, k, i) \times \Pr(\tau|k, i)$, the ratio of marginal likelihoods can be expressed as the ratio between the prior and the posterior at $\tau = 0$, i.e.,

$$\frac{\Pr(\mathcal{D}|\mathcal{H}_1, k, i)}{\Pr(\mathcal{D}|\mathcal{H}_0, k, i)} = \frac{\Pr(\tau = 0|k, i)}{\Pr(\tau = 0|\mathcal{D}, k, i)} = \Pr(\tau = 0|\mathcal{D}, k, i)^{-1}, \quad (17)$$

assuming an exponential prior in the numerator. Plugging (17) into (15) and solving, we finally get

$$\Pr(\mathcal{H}_1|\mathcal{D}, k, i) = \left[1 + \frac{\Pr(\tau = 0|\mathcal{D}, k, i)}{\text{Odds}(\mathcal{H}_1|k, i)} \right]^{-1}. \quad (18)$$

The probability (18) expresses the significance of the mode \hat{m}_i in the k -modal pdf \tilde{f}_k . The classical theory of Bayes factors for hypothesis testing establishes some reference values to interpret (18). See Kass and Raftery (1995, Section 3.2) for a scale in terms of (17). This methodology gives the benefit of the doubt to the null hypothesis \mathcal{H}_0 , requiring a value of (18) well above 0.50 to reject it. Such conservatism would also be justified in our case for parsimony.

The probabilities (18) for the left, centre and right modes in Fig. 6b are 0.69, 0.74 and 0.99, respectively, assuming all the prior odds equal one. These results agree with our intuition that the left mode is relatively weak, and only that to the right is beyond doubt.

Applying the same procedure on the pdf in Fig. 1c of the Hidalgo problem, we obtain probabilities from left to right: 0.63, 0.99, 0.83, 0.96, 0.91, 0.51 and 0.75. According to the scale in Kass and Raftery (1995), only the second to fifth modes would be significant, yielding four modes instead of the original seven. It is easy to see why by looking at Fig. 1a. The modes at 7 and 12 are *fractured*, while few data points support the one at 13. From this one-dimensional mode testing perspective, BTS would agree with the four-mode solution by Ameijeiras-Alonso et al. (2018).

Notwithstanding, limiting our analysis to the probabilities (18) has several drawbacks. Setting a decision threshold might be too rigid and arbitrary, and, more importantly, discarding modes on the grounds of significance equates to forgetting the global results making the local analysis (18) possible. In fact, for the Hidalgo problem, the previous stages of BTS led unequivocally to seven modes.

We propose to round BTS off by combining the *global* probabilities obtained in Section 3.3 with new *scores* for each k based on (18). Let $\Pr(\mathcal{H}_1|k, \mathcal{D})$ be the new score for the k hypothesis, representing its *overall* significance. If the latter plays the part of the likelihood and we take $\Pr(k|\mathcal{D})$ as prior probabilities, the ‘‘Bayesian update’’ yields the posterior $\Pr(k|\mathcal{H}_1, \mathcal{D}) \propto \Pr(\mathcal{H}_1|k, \mathcal{D}) \times \Pr(k|\mathcal{D})$, assuming that $\Pr(k|\mathcal{H}_1, \mathcal{D}) = 0$ whenever $\Pr(k|\mathcal{D}) = 0$. The latter posterior can be seen as the sum of two compositional vectors. If $\Pr(\mathcal{H}_1|k, \mathcal{D}) = 0$ for all k , we should take $\Pr(k|\mathcal{H}_1, \mathcal{D}) = \Pr(k|\mathcal{D})$. See Egozcue and Pawlowsky-Glahn (2018) for a similar treatment of likelihoods as general *evidence functions*.

Finally, the *refined* estimator variant of BTS is defined analogously to (13) as

$$\hat{k}_{\text{BTS},2} = \arg \max_{k \in \mathbb{N}} \Pr(k|\mathcal{H}_1, \mathcal{D}). \quad (19)$$

If there is only one $k \in \mathbb{N}$ such that $\Pr(k|\mathcal{D}) > 0$, the estimators (13) and (19) coincide. Therefore, in the case of the Hidalgo problem, despite some modes being non-significant, we have $\hat{k}_{\text{BTS},2} = \hat{k}_{\text{BTS},1} = 7$.

There are many ways to aggregate all the probabilities (18) into a single score. We propose taking the *harmonic mean*. Amongst the Pythagorean means, it is the most sensitive to the lower outliers while stable against the higher ones. Let us define $\text{Odds}(\mathcal{H}_1|k)$ as the harmonic mean of the prior odds for each of the k modes in \tilde{f}_k , i.e., $\text{Odds}(\mathcal{H}_1|k) = k / \sum_{i=1}^k \text{Odds}(\mathcal{H}_1|k, i)^{-1}$. Also, define the mixture

$$\Pr(\tau|k, \mathcal{D}) = \sum_{i=1}^k w_i \Pr(\tau|\mathcal{D}, k, i), \text{ where } w_i = \frac{\text{Odds}(\mathcal{H}_0|k, i)}{\sum_{j=1}^k \text{Odds}(\mathcal{H}_0|k, j)}.$$

Then, the harmonic mean $\Pr(\mathcal{H}_1|k, \mathcal{D}) = k / \sum_{i=1}^k \Pr(\mathcal{H}_1|\mathcal{D}, k, i)^{-1}$ satisfies

$$\Pr(\mathcal{H}_1|k, \mathcal{D}) = \left[1 + \frac{\Pr(\tau = 0|k, \mathcal{D})}{\text{Odds}(\mathcal{H}_1|k)} \right]^{-1},$$

making it a generalisation of (18) for k higher than one.

4. CASE STUDY

Pitchers are a central part of baseball. They develop a comprehensive throw repertoire that varies in speed, spin and target. Thus, classifying a pitch is challenging, even for a well-trained eye. Nonetheless, to a first approximation, speed takes considerable variability while widely recognised as the main asset of a pitcher. Therefore, let us study pitching from the univariate perspective of speed.

Knowing the *arsenal* of the opposing pitcher increases the chances of a batter hitting the ball. In particular, we can gain valuable knowledge from the speed modes. The larger the NoM, the greater the unpredictability of the pitcher. A scouting report could advise that batters focus their pre-game training and in-game strategy on specific ball speeds corresponding to the modes.

We will look at the pitching speeds of *Major League Baseball* (MLB) top player Shohei Ohtani in the 2022 season. See the SM (Chacón and Fernández Serrano, 2023) for further details on the data. Fig. 7a is a bar chart of the underlying pitches, omitting some outliers below 70 miles per hour (mph). The 2,626-point sample consists of speed values reported up to 0.1 mph, making up a discretised dataset. Hence, extra smoothing will be induced in BTS, as mentioned in the SM (Chacón and Fernández Serrano, 2023). A large compositional spline space dimension $d = 32$ will be employed, as well.

The official interpretation of the pitches by the MLB comprises four modes. Three can be identified with specific pitch types: the *curveball* (with an average of 78 mph), the *slider* (85 mph) and the *fastball* (97 mph). The last mode, located at approximately 90 mph, emerges from a mix of *changeups* and *cutters*. Several preliminary pdf models are depicted in Fig. 7b. The PI_0 -variant of the KDE points out four modes, whereas PI_1 eludes the 90-mph mode. The parametric Gaussian mixture model is the least expressive with two modes, missing the latter plus the curveball.

The intermediate results of BTS are qualitatively very similar to the examples in Section 3. We will go straight to the final results from the selection and testing stages and refer the reader to the SM (Chacón and Fernández Serrano, 2023) for the rest. Depending on the prior probabilities $\Pr(k)$, we have both $\Pr(k = 4|\mathcal{D})$ and $\Pr(k = 4|\mathcal{H}_1, \mathcal{D})$ ranging between 0.93 and 0.98. The mode tree weighted with the posterior sample is in Fig. 8a, while the posterior median spline for $k = 4$ is in

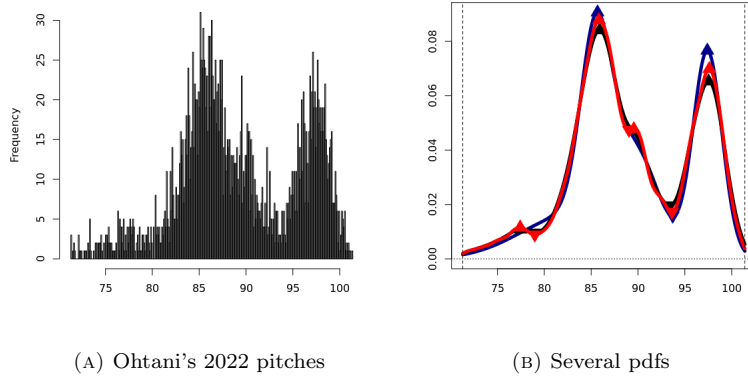


FIG. 7. Shohei Ohtani's 2022 pitching season data. The left-hand side picture shows a bar chart of the sample, consisting of 2,626 pitch speeds greater than or equal to 70 mph. Several pdfs for that sample are shown on the right. Namely, the pdfs are PI_0 (red, 4 modes), PI_1 (black, 3 modes), and a Gaussian mixture (blue, 2 modes).

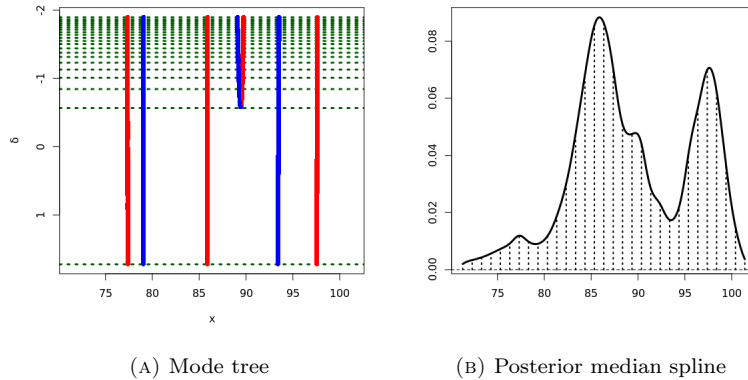


FIG. 8. Results of the BTS method for the MLB case study with the same structure as Fig. 6. The black vertical lines are omitted from the mode tree on the left to enhance readability under a larger sample size. The dimension of the posterior median model with four modes is 32.

Fig. 8b. The modes of the latter pdf are located at 77.4, 85.9, 89.7 and 97.6 mph, having significance probabilities of 0.85, 0.99, 0.62 and 0.99, respectively.

5. SIMULATION STUDY

This section demonstrates the effectiveness of our proposal in a thorough comparison with other well-established techniques. As we will see, BTS is a top-tier method according to an overall ranking aggregating results from a broad array of test-beds. We will also examine under what circumstances each procedure performs best and worst and analyse the distribution of the predictions. The reader is referred to the SM (Chacón and Fernández Serrano, 2023) for extra auxiliary results and setup details.

5.1. **Setup.** The experimental design is fully described in the following lines.

Methods. Seven variants of BTS are tested in this simulation study:

- BTS0: The *raw* BTS estimator (8).
- BTS1S: The *processed* BTS estimator (13) with $\Pr(k)$ estimated from \mathcal{S} .
- BTS1J: The *processed* BTS estimator (13) with $\Pr(k) = \int_{\Delta_k} \Pr(\delta) d\delta$.
- BTS1U: The *processed* BTS estimator (13) with $\Pr(k) \propto 1$.
- BTS2S: The *refined* BTS estimator (19) with $\Pr(k)$ estimated from \mathcal{S} .
- BTS2J: The *refined* BTS estimator (19) with $\Pr(k) = \int_{\Delta_k} \Pr(\delta) d\delta$.
- BTS2U: The *refined* BTS estimator (19) with $\Pr(k) \propto 1$.

When comparing alternative methods, we will focus on BTS2U, which encompasses all four BTS stages and provides competitive results. We refer the reader to the SM (Chacón and Fernández Serrano, 2023) to compare all the different BTS variants. Standard BTS configurations with $d = 22$ basis functions were used in all cases.

The alternative methods considered in this simulation study, which are described and justified in the SM (Chacón and Fernández Serrano, 2023), are the following:

- PI0: The NoM of the KDE with *plug-in* (PI) bandwidth for $r = 0$.
- PI1: The NoM of the KDE with PI bandwidth for $r = 1$.
- PI2: The NoM of the KDE with PI bandwidth for $r = 2$.
- SCV: The NoM of the KDE with *smoothed cross-validation* (SCV) bandwidth.
- STE: The NoM of the KDE with *solve-the-equation* (STE) bandwidth.
- LSCV0: The NoM of the KDE with *least-squares cross-validation* (LSCV) bandwidth for $r = 0$.
- LSCV1: The NoM of the KDE with LSCV bandwidth for $r = 1$.
- LSCV2: The NoM of the KDE with LSCV bandwidth for $r = 2$.
- GM: The NoM of a Gaussian mixture model selected via *Bayesian information criterion*.
- TS: The number of *peaks* of a *taut string* fitted based on Kuiper metrics (Davies and Kovac, 2004).
- SI: The highest NoM that the critical bandwidth test by Silverman (1981) cannot reject at a 0.05 significance level.
- FM: The highest NoM that the critical bandwidth test by Fisher and Marron (2001) cannot reject at a 0.05 significance level.
- EIG: The maximum number of significant KDE modes at a 0.10 significance level, according to Genovese et al. (2016).

Test-beds. We propose as test-beds the $T = 5$ three-modal Gaussian mixtures considered in Ameijeiras-Alonso (2017, pp. 124-125): M21, M22, M23, M24 and M25. They are the most complex models in Ameijeiras-Alonso (2017) and Ameijeiras-Alonso et al. (2018). We refer the reader to the SM (Chacón and Fernández Serrano, 2023) for the definition and plotting of these pdfs.

Experimental design. Each test-bed will be paired with $S = 3$ sample sizes: $n = 100$ (small), $n = 400$ (medium-sized), and $n = 1600$ (large), adding up to $T \times S = 15$ sampling configurations. Then, $m = 200$ replications of the experiment, drawing i.i.d. observations from each combination of test-bed and sample size, will be carried out to obtain significant results, as in Lee (2003).

The results from each sampling configuration will be analysed separately first. For each method M_j , $j \in \{1, \dots, M\}$, and sample \mathcal{D}_i , $i \in \{1, \dots, m\}$, an estimate $\hat{k}_{j,i} \in \mathbb{N}$ of the NoM will be recorded. Comparing the BTS variants, we have $M = 7$, whereas comparing BTS2U with the alternative methods yields $M = 14$. Assuming a ground truth target NoM $k = 3$ for every test-bed model, an outcome $\omega_{j,i} \in \{0, 1\}$

PIO	PI1	PI2	SCV	STE	LSCV0	LSCV1	LSCV2	GM	TS	SI	FM	EIG	BTS2U
1	2	5	1	1	2	2	3	1	6	6	4	6	1

TABLE 1. Global ranking.

is derived taking $\omega_{j,i} = 1$, if $\hat{k}_{j,i} = k$, and $\omega_{j,i} = 0$, otherwise. Then, the *accuracy* of the j -th method is $\varpi_j = m^{-1} \sum_{i=1}^m \omega_{j,i}$.

Two methods M_μ and M_ν are confronted by comparing the outcome sequences $(\omega_{\mu,i})_{i=1}^m$ and $(\omega_{\nu,i})_{i=1}^m$. One method is ranked ahead if (i) its accuracy is greater than that of the other *and* (ii) both methods provide significantly different performances according to McNemar’s test (McNemar, 1947) using a standard significance level $\alpha = 0.01$. Otherwise, both methods shall be ranked the same. The $M(M-1)/2$ pairwise orderings are then aggregated using the Kemeny distance approach in Amodio et al. (2016), which computes a *median* ranking, possibly including ties among the individual method ranks. If there is no unique solution, we propose aggregating all the resulting rankings via simple component-wise rank averaging, a typical default procedure mentioned in Amodio et al. (2016).

After computing the intermediate rankings $\mathcal{R}_1, \dots, \mathcal{R}_{T \times S}$, a final aggregation using the previous procedure, consisting of a median consensus ranking and averaging in case of multiple solutions, yields a unique global ranking \mathcal{R} , possibly with ties.

5.2. Results. We will now look at the results following the previous setup and methodology. By convention, the best position is 1 in all rankings, as in Amodio et al. (2016).

Before diving into the results, we urge the reader to take them cautiously. As warned by Lee (2003), these are only simulations, spanning a small and simplified piece of the problem. Moreover, there is no canonical way of analysing and aggregating the results (see, for instance, Cao et al., 1994, Section 3.2).

Global ranking. The global ranking \mathcal{R} is presented in Table 1. As we can see, BTS2U belongs in the same top-ranked group as the parametric GM and the KDEs PIO, SCV and STE, all of them generic direct approaches. In the second place, we find two LSCV variants, LSCV0 and LSCV1, and the first-order PI version, PI1. Next, LSCV2, the remaining LSCV, holds the third rank. The bottom three positions gather all the methods tailored explicitly for mode estimation. Coming fourth and fifth, we have the best performer of the two test-based approaches, FM, and the last member of the PI family, PI2. Finally, ranking at the bottom appears the other test, SI, alongside two methods genuinely related to modes, TS and EIG.

The same exact final ranking is obtained for various significance levels in McNemar’s test, aside from our reference value $\alpha = 0.01$, evidencing the robustness of our conclusions.

The results in Table 1 may look counterintuitive. Direct non-specific methods perform better than those specifically designed for modality assessment. In that sense, customary KDE bandwidth selectors for the pdf usually provide the correct answer, matching the performance of GM, which, given the nature of the considered test-beds, can be seen as an upper limit in performance.

The FM method by Fisher and Marron (2001) comes as the top-qualified classic approach, outmatching SI, the original critical bandwidth proposal by Silverman (1981). In turn, the poor results of TS and EIG are especially striking, demonstrating that too much parsimony might not work well in practice.

		PI0	PI1	PI2	SCV	STE	LSCV0	LSCV1	LSCV2	GM	TS	SI	FM	EIG	BTS2U
M21	100	2	3	3	2	1	1	1	2	2	3	3	3	3	2
M21	400	2	4	6	2	1	1	2	3	2	6	6	5	6	2
M21	1600	2	4	6	2	2	3	4	5	1	9	7	5	8	2
M22	100	3	7	8	5	2	4	6	7	6	8	8	7	8	1
M22	400	1	1	6	1	2	5	3	4	1	7	2	1	7	2
M22	1600	2	1	1	2	4	8	6	6	1	7	1	1	5	3
M23	100	2	4	6	2	1	2	2	3	1	7	7	5	7	2
M23	400	2	1	3	2	5	7	6	6	1	6	6	4	7	4
M23	1600	4	2	1	5	7	8	8	7	1	3	1	3	6	6
M24	100	3	4	5	3	1	3	3	3	5	5	5	5	3	2
M24	400	1	2	3	1	1	2	2	2	3	3	3	3	2	1
M24	1600	1	1	4	1	2	5	2	2	5	5	7	6	3	1
M25	100	2	5	6	2	1	2	3	4	6	8	8	5	7	3
M25	400	1	3	8	1	1	2	4	6	7	10	9	5	10	1
M25	1600	2	1	2	2	2	3	3	4	1	6	4	2	5	2

TABLE 2. Intermediate rankings by test-bed and sample size configuration.

Intermediate rankings. The rankings $\mathcal{R}_1, \dots, \mathcal{R}_{T \times S}$ are reported in Table 2. See the SM (Chacón and Fernández Serrano, 2023) for an in-depth commentary with plots.

As we see, no method performs uniformly better than the rest across all settings. Nonetheless, the intermediate rankings confirm the superiority of the top-ranked methods in Table 1: GM, PI0, SCV, STE and our BTS2U. They rank high most of the time and, more importantly, consistently escape from the bottom position. Indeed, at least one of these methods ranks first in each considered case. Especially worth mentioning is the M22-100 setting, where BTS2U ranks ahead of the rest.

Beyond the top-tier methods, Table 2 shows that the global ranking is quite unfair with PI1, as PI1 lands the first position once more than PI0 and SCV. The reason why PI1 ranks globally worse lies in its uneven performance. Small datasets particularly harm PI1. Also, PI1 struggles with M21, regardless of the sample size. As we can see in the SM (Chacón and Fernández Serrano, 2023), the slight middle mode of M21 poses serious problems for the over-smoothing strategy of PI1.

6. DISCUSSION

BTS faces estimating the NoM inspired by some little-known aspects of the problem. The need for structure diagnosed by Donoho (1988) is implemented through a combination of KDEs (Wand and Jones, 1995) and compositional splines (Machalová et al., 2020). Subsequently, the Bayesian inference machinery (Bernardo, 1994) offers standard procedures to balance data fitting and model complexity, incorporate expert knowledge and assess the uncertainty of the results. Finally, global model selection (Wasserman, 2000) and local testing (Minnotte and Scott, 1993) allow for a holistic view of modality.

We follow a strategic *divide-and-conquer* approach similar to that suggested by Good and Gaskins (1980). An exploration phase via MCMC enforces regularity in the solutions, penalising curvature and multimodality. A numerous sample of candidate compositional splines is summarised using SFPCA (Hron et al., 2016), obtaining a one-parameter model that retains the essential modal features. Then, the Bayesian update weighs the probabilities of each k -modality hypothesis in an encompassing prior (Klugkist et al., 2005), producing a characteristic median compositional spline for each k . Next, each representative pdf has its k modes tested using a Bayesian Savage-Dickey scheme (Wagenmakers et al., 2010) with data in the excess mass region of the mode. Lastly, the global and local scores are *summed* to determine the most likely k .

Traditional approaches for modality either offer a lot of sparse information, such as mode trees (Minnotte and Scott, 1993) or SiZer (Chaudhuri and Marron, 1999), or act as a *black box* outputting an actionable but cryptic p-value, such as the critical bandwidth test (Fisher and Marron, 2001; Silverman, 1981). BTS delivers traceable and interpretable intermediate products, providing a fuzzy but straightforward result. The h - α scatter plot in Fig. 3 studying modality from a twofold perspective represents a legitimate innovation for mode exploration. Then, Fig. 6a and Fig. 8a are upgraded mode trees with several advantages: sensible prescribed upper and lower bounds, a well-behaved natural parameter without resorting to the logarithmic scale, and a posterior pdf that allows placing cue quantiles in the parameter axis. Additionally, the final decision for k is supported on a tangible pdf, as in Fig. 8b.

Several practical experiences support BTS. Our seven-mode result for the Hidalgo problem is well-grounded on likelihood. There are also qualitative reasons, such as the modes approximately appearing at regular integer values, a much human-like trait. On the other hand, the four-mode solution of Ameijeiras-Alonso et al. (2018), for instance, demands a similar smoothing to PI1, which we know does not perform well on medium-sized samples with subtle features, according to Section 5. Also, such a smoothing level would imply that the stamp manufacturing process had high variability, including a strange *shoulder* in the density of the thickness distribution. As for the MLB case study, our four-mode solution agrees with the official interpretation of the MLB. Interestingly, our results grant a small probability of having only three modes, with a weak significance score for the dubious changeup-cutter mode. Unlike our method, the Gaussian mixture approach failed conservatively in both real settings since, contrary to the simulation study, non-Gaussianity and discretisation were present.

The simulation study unveils highly unexpected findings. The traditional methods for modality, e.g., FM, SI or TS, fall deeply in the rankings behind generic plug-in KDE-based estimators such as PI0 and STE. Hypothesis testing methods underperform if evaluated far from their restricted theoretical framework, which leads us to question their actual value in practice when they are sequentially employed to estimate the NoM. Moreover, we have not observed the typical asymptotic accuracy boost of nonparametric methods. In turn, the taut string TS is conservatively biased, recalling the approach by Donoho (1988) for calculating a lower confidence bound for the NoM. As for our proposal, even though the BTS2U variant of BTS is a top-tier method, there is still room for accuracy improvement, perhaps using auxiliary techniques such as ensembles or bootstrapping.

If the user has to make a *blindfold* decision, our overall recommendation for estimating the NoM is PI0 based on accuracy, robustness, versatility, simplicity and low computational cost. The empirical evidence generally supports the sound theory behind it. With large samples, looking at PI1 should pay off, as well. Nevertheless, analysts usually prefer analysing data rather than simply *hitting a button* and reporting some output. For them, BTS offers valuable resources with similar accuracy to PI0. In this respect, BTS would benefit from a graphical interface for the analysts to work interactively and efficiently access all the available information. Additionally, beyond the NoM, BTS could serve as a more elaborate and dependable version of PI0 for pdf estimation in the context of bounded data.

ACKNOWLEDGEMENTS

The research of the first author has been supported by the MICINN grants PID2019-109387GB-I00 and PID2021-124051NB-I00. The second author would like to thank Professor Amparo Baíllo Moreno for her advice as a doctoral counsellor at

the Autonomous University of Madrid. Finally, we thank an associate editor and two anonymous reviewers for their helpful comments.

REFERENCES

- AMELJEIRAS-ALONSO, J. (2017). “Assessing simplifying hypotheses in density estimation”. PhD thesis. Universidade de Santiago de Compostela.
- AMELJEIRAS-ALONSO, J., CRUJEIRAS, R. M., and RODRÍGUEZ-CASAL, A. (2018). Mode testing, critical bandwidth and excess mass. *TEST* **28**, 900–19.
- AMELJEIRAS-ALONSO, J., CRUJEIRAS, R. M., and RODRÍGUEZ-CASAL, A. (2021). Multimode: an R package for mode assessment. *Journal of Statistical Software* **97**.
- AMODIO, S., D’AMBROSIO, A., and SICILIANO, R. (2016). Accurate algorithms for identifying the median ranking when dealing with weak and partial rankings under the Kemeny axiomatic approach. *European Journal of Operational Research* **249**, 667–76.
- ARIAS-CASTRO, E. and JIANG, H. (2022). Fitting a multi-modal density by dynamic programming. *arXiv preprint*.
- BERNARDO, J. M. (1994). Bayesian statistics. *Probability and statistics*. Vol. 2, 345–407.
- CAO, R., CUEVAS, A., and GONZÁLEZ-MANTEIGA, W. (1994). A comparative study of several smoothing methods in density estimation. *Computational Statistics & Data Analysis* **17**, 153–76.
- CHACÓN, J. E. (2015). A population background for nonparametric density-based clustering. *Statistical Science* **30**, 518–32.
- CHACÓN, J. E. (2018). Mixture model modal clustering. *Advances in Data Analysis and Classification* **13**, 379–404.
- CHACÓN, J. E. (2020). The modal age of statistics. *International Statistical Review* **88**, 122–41.
- CHACÓN, J. E. and DUONG, T. (2013). Data-driven density derivative estimation, with applications to nonparametric clustering and bump hunting. *Electronic Journal of Statistics* **7**, 499–532.
- CHACÓN, J. E. and FERNÁNDEZ SERRANO, J. (2023). *Supplementary material to “Bayesian taut splines for estimating the number of modes”*.
- CHAUDHURI, P. and MARRON, J. S. (1999). SiZer for exploration of structures in curves. *Journal of the American Statistical Association* **94**, 807–23.
- CHAUDHURI, P. and MARRON, J. S. (2002). Curvature vs. slope inference for features in nonparametric curve estimates. *Unpublished manuscript*.
- CHENG, M.-Y. and HALL, P. (1998). Calibrating the excess mass and dip tests of modality. *Journal of the Royal Statistical Society: Series B (Statistical Methodology)* **60**, 579–89.
- CHENG, M.-Y. and HALL, P. (1999). Mode testing in difficult cases. *The Annals of Statistics* **27**, 1294–315.
- CUEVAS, A., FEBRERO, M., and FRAIMAN, R. (2000). Estimating the number of clusters. *Canadian Journal of Statistics* **28**, 367–82.
- DAVIES, L., GATHER, U., NORDMAN, D., and WEINERT, H. (2009). A comparison of automatic histogram constructions. *ESAIM: Probability and Statistics* **13**, 181–96.
- DAVIES, L. and KOVAC, A. (2004). Densities, spectral densities and modality. *The Annals of Statistics* **32**, 1093–136.
- DONOHO, D. L. (1988). One-sided inference about functionals of a density. *The Annals of Statistics* **16**, 1390–420.
- DÜMBGEN, L. and WALTHER, G. (2008). Multiscale inference about a density. *The Annals of Statistics* **36**, 1758–85.
- EGOZCUE, J. J. and PAWLOWSKY-GLAHN, V. (2018). Evidence functions: a compositional approach to information. *SORT. Statistics and Operations Research Transactions*, 101–24.
- FISHER, N. I., MAMMEN, E., and MARRON, J. S. (1994). Testing for multimodality. *Computational Statistics & Data Analysis* **18**, 499–512.
- FISHER, N. I. and MARRON, J. S. (2001). Mode testing via the excess mass estimate. *Biometrika* **88**, 499–517.
- GENOVESE, C., PERONE-PACIFICO, M., VERDINELLI, I., and WASSERMAN, L. (2016). Non-parametric inference for density modes. *Journal of the Royal Statistical Society: Series B (Statistical Methodology)* **78**, 99–126.
- GOOD, I. J. and GASKINS, R. A. (1980). Density estimation and bump-hunting by the penalized likelihood method exemplified by scattering and meteorite data. *Journal of the American Statistical Association* **75**, 42–56.
- HALL, P. and YORK, M. (2001). On the calibration of Silverman’s test for multimodality. *Statistica Sinica* **11**, 515–36.
- HARTIGAN, J. A. and HARTIGAN, P. M. (1985). The dip test of unimodality. *The Annals of Statistics* **13**, 70–84.

- HRON, K., MENAFOGLIO, A., TEMPL, M., HRŮZOVÁ, K., and FILZMOSER, P. (2016). Simplicial principal component analysis for density functions in Bayes spaces. *Computational Statistics & Data Analysis* **94**, 330–50.
- IZENMAN, A. J. and SOMMER, C. J. (1988). Philatelic mixtures and multimodal densities. *Journal of the American Statistical Association* **83**, 941–53.
- KASS, R. E. and RAFTERY, A. E. (1995). Bayes factors. *Journal of the American Statistical Association* **90**, 773–95.
- KLUGKIST, I., KATO, B., and HOIJTINK, H. (2005). Bayesian model selection using encompassing priors. *Statistica Neerlandica* **59**, 57–69.
- LEE, T. C. M. (2003). Smoothing parameter selection for smoothing splines: a simulation study. *Computational Statistics & Data Analysis* **42**, 139–48.
- MACHALOVÁ, J., TALSÁ, R., HRON, K., and GÁBA, A. (2020). Compositional splines for representation of density functions. *Computational Statistics* **36**, 1031–64.
- MAMMEN, E., MARRON, J. S., and FISHER, N. I. (1992). Some asymptotics for multimodality tests based on kernel density estimates. *Probability Theory and Related Fields* **91**, 115–32.
- MARRON, J. S. and SCHMITZ, H.-P. (1992). Simultaneous density estimation of several income distributions. *Econometric Theory* **8**, 476–88.
- MCNEMAR, Q. (1947). Note on the sampling error of the difference between correlated proportions or percentages. *Psychometrika* **12**, 153–7.
- MINNOTTE, M. C. (1997). Nonparametric testing of the existence of modes. *The Annals of Statistics* **25**, 1646–60.
- MINNOTTE, M. C., MARCHETTE, D. J., and WEGMAN, E. J. (1998). The bumpy road to the mode forest. *Journal of Computational and Graphical Statistics* **7**, 239–51.
- MINNOTTE, M. C. and SCOTT, D. W. (1993). The mode tree: a tool for visualization of nonparametric density features. *Journal of Computational and Graphical Statistics* **2**, 51–68.
- MULLER, D. W. and SAWITZKI, G. (1991). Excess mass estimates and tests for multimodality. *Journal of the American Statistical Association* **86**, 738–46.
- POLONIK, W. (1995a). Density estimation under qualitative assumptions in higher dimensions. *Journal of Multivariate Analysis* **55**, 61–81.
- POLONIK, W. (1995b). Measuring mass concentrations and estimating density contour clusters—an excess mass approach. *The Annals of Statistics* **23**, 855–81.
- SILVERMAN, B. W. (1981). Using kernel density estimates to investigate multimodality. *Journal of the Royal Statistical Society: Series B (Statistical Methodology)* **43**, 97–9.
- SOMMERFELD, M., HEO, G., KIM, P., RUSH, S. T., and MARRON, J. S. (2017). Bump hunting by topological data analysis. *Stat* **6**, 462–71.
- WAGENMAKERS, E.-J., LODEWYCKX, T., KURIYAL, H., and GRASMAN, R. (2010). Bayesian hypothesis testing for psychologists: a tutorial on the Savage–Dickey method. *Cognitive Psychology* **60**, 158–89.
- WAND, M. P. and JONES, M. C. (1995). *Kernel smoothing*. Springer US.
- WASSERMAN, L. (2000). Bayesian model selection and model averaging. *Journal of Mathematical Psychology* **44**, 92–107.

This page intentionally left blank.

Supplementary material

The following *appendices* are provided as *supplementary material* to the manuscript *Bayesian taut splines for estimating the number of modes*. Equation numbers refer to the manuscript. The numbers for new equations are prefixed. References are included at the end. Notation and acronyms are reused from the manuscript.

Appendix A and Appendix B explain the philosophy and implementation details of BTS. Then, Appendix C, Appendix D, and Appendix E expand on the case and simulation studies. Finally, Appendix F and Appendix G discuss relevant theoretical and practical issues.

APPENDIX A. MOTIVATION

The following lines motivate the design of BTS in Section 3 along three axes.

Structure. Researchers have mainly tackled modality through nonparametric approaches, for parametric ones are deemed too rigid (Ameijeiras-Alonso, 2017). However, the work by Donoho (1988) suggests that modality is impossible to *tame* under weak nonparametric regularity assumptions. For that matter, the quest for modes has the existence of a pdf as a prerequisite, something we cannot test empirically (Donoho, 1988).

Consequently, some structure seems due in the study of modes, balancing data fitting and model complexity. This policy is exhibited by Davies et al. (2009) in the context of histograms or Good and Gaskins (1980) with Fourier series. In this respect, smoothing splines are the right tool, allowing restrained flexibility (Eilers and Marx, 1996; Hron et al., 2016; Machalová et al., 2020). BTS thus targets a compromise between both dimensions by blending KDEs and compositional splines.

On the one hand, KDEs serve as a *scaffold* for splines, guiding high-dimensional fitting more efficiently than customary histograms (Eilers and Marx, 1996; Machalová et al., 2020). On the other, the comparatively rigid structure of splines and their built-in curvature penalisation (Machalová et al., 2020) represent a *har-ness* for KDEs, preventing spurious modes. Additionally, curvature penalisation mitigates the effect of the KDE having a single global bandwidth h (Minnotte and Scott, 1993). Finally, splines allow for a deeper analysis and simplification of the modal structure via dimensionality reduction (Hron et al., 2016).

Bayesian inference. Mode estimation reveals philosophical issues excellently handled by Bayesian inference (Bernardo, 1994). Emphasising *frequentist* population-wide properties over actual data is unrealistic in some cases. The Hidalgo problem is a paradigmatic example since the stamps are no longer issued. In turn, the Bayesian approach is the right choice when data is scarce, and any information, such as philately expert knowledge, could be helpful.

Bayesian inference provides *soft* solutions, quantifying their uncertainty (Bernardo, 1994). Current methods cannot assign a probability to each k -modality hypothesis. For instance, hypothesis testing procedures report p-values limited to the null hypothesis (Wagenmakers et al., 2010). Meanwhile, mode trees (Minnotte, 1997; Minnotte et al., 1998; Minnotte and Scott, 1993) and SiZer (Chaudhuri and Marron, 1999), though incorporating mechanisms to assess the uncertainty, fall short of providing actionable answers. By contrast, the Bayesian framework excels at operating with probabilities, offering standard hypothesis selection tools (Kass and Raftery, 1995; Klugkist et al., 2005; Spiegelhalter et al., 2014; Wagenmakers et al., 2010; Wasserman, 2000).

The subjective nature of modes particularly suits Bayesian methods. The wide array of graphical methods (Chaudhuri and Marron, 1999, 2002; Minnotte, 1997; Minnotte et al., 1998; Minnotte and Scott, 1993) evidence that the human eye,

aided by a computer, better appreciates such features (Good and Gaskins, 1980). Consequently, the usual criticism that Bayesian inference is not objective loses force (Bernardo, 1994). Moreover, Bayesian tools are less prone to overfitting since they examine a range of plausible outcomes rather than isolated optima. This inherent *parsimony* (Wagenmakers et al., 2010) will be valuable against spurious modes.

Holism. Modes are challenging for their dual local and global nature. They are defined via a local property of the pdf, but, at the same time, that pdf is built from disconnected data. In that sense, modes are *emergent* phenomena.

BTS aims to combine both perspectives. During the first three stages, the mode concept helps build candidate pdfs. Then, at the fourth stage, the representative pdfs of each modality hypothesis have their modes tested individually using neighbouring data, yielding *significance* scores.

The penalised likelihood approach by Good and Gaskins (1980) and mode trees (Minnotte and Scott, 1993) also include local testing mechanisms after global fitting. Our proposal merges the global and local probabilities into a single result, obtaining a holistic view of modality.

APPENDIX B. IMPLEMENTATION

The following lines discuss the implementation of the BTS method in Section 3.

B.1. Hyperparameter tuning. BTS requires setting several configurations. We comment here on how this can be done in practice with attention to the data.

Prior design. The parametric design (7) of the prior in the exploration stage of BTS was left unexplained. Let us now go deeper into the underlying principles and experiences.

The choice of beta distribution for $1 - \alpha$ is conventional when $\alpha \in (0, 1)$. Fixing $\alpha = 1$ makes the pdf diverge at zero, while $\beta_{1-\alpha}$ controls its expected value through $\mathbb{E}[1 - \alpha] = (1 + \beta_{1-\alpha})^{-1}$. Next, the rationale behind the bandwidth distribution lies in the logarithmic scale, known for improving the appreciation of the KDE changes in mode trees (Minnotte and Scott, 1993). Assuming a normal distribution for $\log h$ with location μ_h and scale σ_h yields maximum entropy and allows focusing on a suitable region of the mode tree. Moreover, preliminary simulations studying critical bandwidths and the posterior $\Pr(h, \alpha | \mathcal{D})$ confirm that the log-normal provides a good approximation. On the other hand, the distributions of k and ξ have been selected to penalise complexity. In the case of k , the Poisson distribution with mean one favours unimodality. For ξ , the exponential pulls the curvature towards zero, leaving control over the mean via $\mathbb{E}[\xi] = \lambda_\xi^{-1}$.

Imposing hyperpriors on (7) would make the MCMC heavier. We propose choosing the hyperparameters empirically. Taking $\beta_{1-\alpha} = 99$ yields $\mathbb{E}[\alpha] = 0.99$, which works well in practice. In turn, for μ_h , σ_h and λ_ξ , we first recommend estimating two tentative values, say $h_1 < h_2$, from distinct bandwidth selectors. Imposing $\log h$ to enclose a central probability $\Phi(\sigma) - \Phi(-\sigma)$ between $\log h_1$ and $\log h_2$, where Φ is the standard univariate Gaussian cdf and $\sigma > 0$, implies $\mu_h = \log \sqrt{h_1 h_2}$ and $\sigma_h = \sigma^{-1} \log \sqrt{h_2/h_1}$. On the other hand, if ξ_1 and ξ_2 are the curvatures of \hat{f}_{h_1} and \hat{f}_{h_2} in the sense of (4), respectively, taking $\lambda_\xi^{-1} = (\xi_1 + \xi_2)/2$ produces a λ_ξ that is the harmonic mean of the λ parameters corresponding to ξ_1 and ξ_2 .

The recommended bandwidth selectors for calculating h_1 and h_2 belong to the PI family of methods PI_r , targeting the r -th derivative for $r = 0, 1, 2$ (Chacón and Duong, 2013). These are robust in an asymptotic sense, avoiding overfitting to \mathcal{D} . Namely, we propose taking $(h_1, h_2) = (h_{\text{PI}_0}, h_{\text{PI}_1})$ in a general setting. For

severely discretised data, $(h_1, h_2) = (h_{\text{PI}_1}, h_{\text{PI}_2})$ offers an extra *shield* against spurious modes. In both cases, we propose $\sigma = 1$ to leave room for exploration beyond (h_1, h_2) . All in all, the previous configurations are somewhat conservative but conform to the regularising goal of the prior $\Pr(h, \alpha)$.

Other configurations. We recommend the *deviance information criterion* (DIC) (Spiegelhalter et al., 2014) to assess the optimal spline dimension d and knot placement strategy, fixing the spline degree to $r = 3$. Too small d will produce too low likelihood values, whereas a too large d will increase the *effective* number of parameters, i.e., the model complexity. The DIC will generally advise against both extremes. Typical values for d are 22 or 32 (i.e., 21 or 31 knots), depending on the intricacies of the data, far from the hundreds of Fourier series terms in Good and Gaskins (1980).

Generally, the grid size m is far less critical than d and can be held to a constant value such as $m = 1001$. The larger the m , the more accurate the spline approximation but the higher the computational cost.

B.2. Simulation. BTS strongly relies on MCMC (Bernardo, 1994). In all three Bayesian inference steps in Section 3, the updated parameters have different support than \mathbb{R} . Sampling directly from those posteriors would lead to abnormally low acceptance rates in MCMC.

In the case of $\Pr(h, \alpha|\mathcal{D})$, we recommend applying the change of variables $\bar{h} = \log h$, $\bar{\alpha} = \Phi^{-1}(\alpha)$ to obtain the posterior $\Pr(\bar{h}, \bar{\alpha}|\mathcal{D}) = \Pr(h, \alpha|\mathcal{D}) \cdot e^{\bar{h}} \cdot \phi(\bar{\alpha})$. Then, we can sample from $(\bar{h}, \bar{\alpha})$ and obtain \mathcal{S} after undoing the change of variables. Similarly, for $\Pr(\delta|\mathcal{D})$, we propose taking $\bar{\delta} = \Phi^{-1}[(\delta - \delta_{\min})/(\delta_{\max} - \delta_{\min})]$, which has pdf $\Pr(\bar{\delta}|\mathcal{D}) \propto \Pr(\delta|\mathcal{D}) \cdot \phi(\bar{\delta})$. Finally, for $\Pr(\tau|\mathcal{D}, k, i)$, we suggest $\bar{\tau} = \log \tau$, yielding $\Pr(\bar{\tau}|\mathcal{D}, k, i) = \Pr(\tau|\mathcal{D}, k, i) \cdot e^{\bar{\tau}}$.

Finding a good initial state for MCMC by calculating the *maximum a posteriori* estimator through a small optimisation will ensure the proper behaviour of the posterior. This will prevent MCMC from including outliers in the posterior sample: the so-called *burn-in* period observations that are usually removed (Wagenmakers et al., 2010).

B.3. Time complexity. BTS is a compound method. It comprises several stages with algorithms of varied nature, including estimation, optimisation, and simulation. In addition to the intrinsic complexity and size of the input data, each procedure has its configuration options, affecting both the execution time and the precision of the results. On the other hand, most of these algorithms are readily implemented as packages, which eases building BTS from scratch but may lead to small inefficiencies. Considering the above, making a comprehensive time complexity analysis of BTS that honours reality is not easy.

Regarding pdf evaluations, all the Bayesian inferences have complexity $\mathcal{O}(Ns)$, where N is the number of data points, and s is the number of MCMC steps. Except for the testing stage, where N is the number of points in the excess mass region, N coincides with the total sample size n . Then, all the pdfs are compositional splines, which can be efficiently evaluated at a single point using B-splines with complexity $\mathcal{O}(d + r^2)$ (Boor, 1972). However, building the model sometimes has a different cost. In the selection and testing stages, the pdfs (9) and (14) belong to a one-dimensional parametric family, so instantiating the model for each δ and τ is almost immediate. By contrast, in the exploration phase, we must build (6) for each (h, α) , consuming much time. The latter step involves several hyperparameters, deserving careful examination.

First, building the CLR grid of the KDE in (4) depends on the sample size n . Naively evaluating (1) at m points has complexity $\mathcal{O}(nm)$ regarding Gaussian

kernel ϕ evaluations. Even if m is held to a moderate constant value, as indicated above, if n is sufficiently large, the execution time may be unaffordable. Using the concept of *binning*, implemented in the package *ks* (Duong, 2022), we can build a discrete approximation to (1) in $\mathcal{O}(n)$ steps that can be evaluated over the grid in $\mathcal{O}(m \log m)$ steps via the FFT algorithm (Gramacki and Gramacki, 2017). Assuming $m \ll n$, the dominant term is $\mathcal{O}(n)$, vastly improving the naive algorithm.

Secondly, solving for the d compositional spline coordinates in (5) requires computations that no longer depend on the sample size once the m -size grid is formed. See Machalová et al. (2020) for further details. Constructing the final linear system matrix has complexity $\mathcal{O}(md)$ in terms of B-spline evaluations, plus $\mathcal{O}(d^2)$ integral calculations for the total curvature penalty component in (4). Finally, using standard implementations, finding the solution to the $d \times d$ linear system has complexity $\mathcal{O}(d^3)$.

Apart from the Bayesian inferences, there is an analysis phase with SFPCA between the exploration and selection stages. See Section F.1 below for further details on SFPCA. Roughly speaking, SFPCA reduces to vanilla PCA and, subsequently, to solving an eigenvalue problem followed by a linear system over $d \times d$ matrices, yielding a complexity $\mathcal{O}(d^3)$ in both cases.

Beyond the sample size and the rest of the hyperparameters, BTS hides a strong dependency regarding the intricacies of the data. The more *ambiguous* the NoM in the data and the higher the maximum predicted NoM, the more calculations are necessary. In some cases, the computational cost increase is negligible. For instance, if many k values have non-null posterior probability (12), it is more expensive to compute the maximum (13). However, letting K be the maximum $k \in \mathbb{N}$ with non-zero probability after the selection phase, the testing stage consists of $K(K+1)/2$ inferences in the worst-case scenario, a complexity $\mathcal{O}(K^2)$, corresponding to testing the k modes of \tilde{f}_k for $k \in \{1, \dots, K\}$.

As the last remark reminds us, BTS is especially suited for data exploration in an interactive environment, possibly with the assistance of a graphical tool. Employing BTS from start to finish in *batch* mode, as we have done in this paper, evenly demonstrates the value of the proposal compared to other alternatives but misses much of its power. Many of the time complexity issues above can be solved with an expert *hand* making good decisions behind the algorithms. For instance, a low-value d might suffice if spline knots are intelligently placed by hand, dramatically reducing the computational cost. Also, running MCMC chains with as many steps s as we have used here may be unnecessary in practice. Moreover, of course, if analysts are overwhelmed by the complexity of the data, they may use the graphical tool to omit some stages of BTS or discard on the run some modality hypotheses based on expert knowledge.

APPENDIX C. EXTRA CASE STUDY

This annexe completes the exposition of the case study in Section 4.

Data. The pitching data has been retrieved using the R package *baseballr* (Petti and Gilani, 2022). Fig. 9 is taken from the MLB-supported advanced metrics website *BaseballSavant* (Willman, 2023). It shows a mixture pdf model of the pitching speeds by Shohei Ohtani with the four modes advanced in Section 4.

Intermediate results. The results of the exploration phase of BTS are shown in Fig. 10, which is similar to Fig. 3 in the synthetic mixture example from Section 3. Up to 77% of the odds favour three modes, while the remaining 23% correspond to four. The subsequent analysis phase results are gathered in Fig. 11. On one side,



FIG. 9. Mixture pdf model of the pitching speeds by Shohei Ohtani in the 2022 season taken from *BaseballSavant* (Willman, 2023). Pitches of different types are modelled in separate mixture components: *curveballs* (blue), *sliders* (yellow), *changeups* (green), *cutters* (brown), and *fastballs* (red). The overall pdf shows up as the black dashed line.

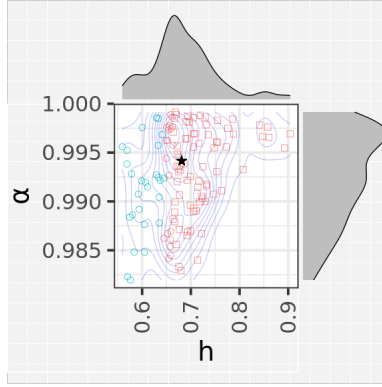


FIG. 10. MCMC sample from the exploration phase of BTS consisting of 120 observations for the MLB case study. The figure follows the structure of Fig. 3. Blue corresponds to four modes (23% of all points) and red to three (77% of the total). Squares and circles refer to three and four modes, respectively.

Fig. 11a shows an even more prominent first PC than Fig. 4a. In turn, Fig. 11b is similar to Fig. 7b in that only $\mu \oplus \delta_{\min} \odot \sigma$ captures the elusive 90-mph mode. In Fig. 12a, the Jeffreys prior for the SFPCA model behind Fig. 11b is qualitatively very similar to Fig. 5a, displaying a mild uniform slope that slightly penalises the fourth mode. The posterior sample for the selection phase appears in Fig. 12b, also having a very similar look to Fig. 5b, definitely leaning the odds towards four modes.

APPENDIX D. EXTRA SETUP

This appendix expands on the simulation study setup in Section 5.1.

D.1. **Methods.** The following lines justify and explain the methods compared in Section 5.1.

Theoretical grounds. The KDE-based methods PI0, PI1, PI2, SCV, STE, LSCV0, LSCV1, LSCV2 and the mixture-based GM are direct *plug-in* approaches, meaning the NoM derives from counting the modes in a fitted pdf model. To do so, we apply the definition in Section 2 of modes as local maxima, restricting the number of pdf evaluations to a sufficiently fine grid over $[a, b]$. Among these direct approaches, GM is parametric, whereas the rest are nonparametric. None of them is tailored explicitly for mode estimation.

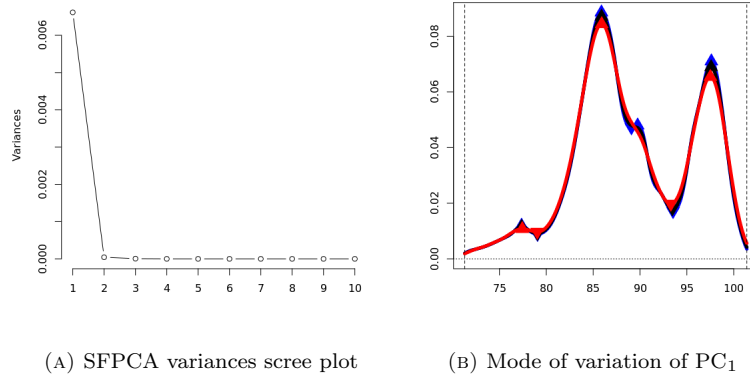


FIG. 11. SFPCA analysis phase results for the MLB case study with the same structure as Fig. 4. The upper bound (red) and the mean (black) pdfs have three modes, while the lower bound (blue) has four.

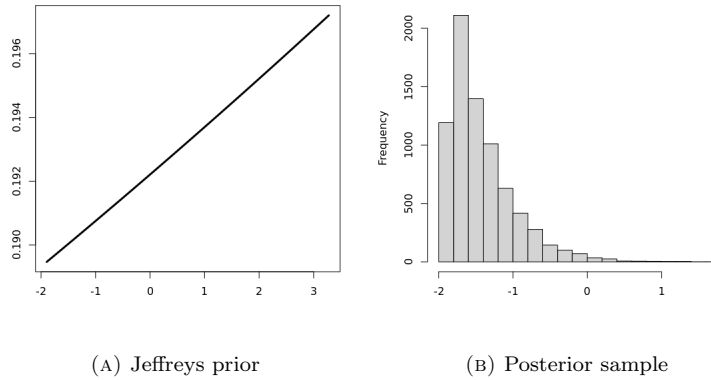


FIG. 12. Second Bayesian inference on the SFPCA model for the MLB case study with the same structure as Fig. 5. The posterior sample to the right comprises 7,437 observations.

The taut string TS method, nonparametric and centred on modality, is also a direct approach but with some additional peculiarities. The continuous and non-uniform definition of mode does not translate well to histogram-like pdfs. In this case, modes should be counted as peaks: the midpoints of bins *taller* than their immediate neighbours. Also, we will interpret a flat taut string, which arguably has no modes, as having modality one, so the minimum NoM will be the same across all direct methods.

Some previous KDEs have been portrayed in Fig. 1b and Fig. 7b. The theory behind the different bandwidth selectors targeting the pdf ($r = 0$) can be found in Wand and Jones (1995). The STE selector is closely related to PI_0 , minimising the same loss function but with a slightly different solution scheme (Wand and Jones, 1995, p. 74). The corresponding extensions for density derivative estimation ($r > 0$) are described in Chacón and Duong (2018). Those were included because of the connection of the first and second derivatives with local maxima (Chaudhuri and Marron, 1999, 2002).

To make a fair comparison with BTS, all the KDEs are equipped with the same outlier-filtering preprocessing step described for BTS in Section 3.1, employing an almost negligible mass threshold of 0.001. Data points belonging to modal regions below that mass are discarded when building the final pdf. The preliminary findings leading to the design of BTS evidenced the extreme sensitivity of KDEs to isolated points when estimating the NoM, a rare risk but with a high impact on the results. The vast majority of such spurious modes generated nearly imperceptible modal regions, easily ignored by the human eye. Therefore, we decided to expand all the outlier-prone methods to match the performance a human would get from them under regular operation. This extra help is unnecessary for the rest.

A second group comprises the mode hypothesis testing methods SI and FM. To obtain the NoM estimate, we iteratively test the null hypothesis that the NoM is less than or equal to k against the alternative of being greater than k , beginning with $k = 1$ and stopping the first time the null hypothesis cannot be rejected. Such an iterative process is customarily used to convert hypothesis testing procedures into estimation ones (Ameijeiras-Alonso et al., 2018, p. 917). The same intermediate significance level $\alpha = 0.05$ is used at every iteration, while the number of bootstrap samples is $B = 500$, being both settings as in Ameijeiras-Alonso et al. (2018).

The excess mass approach is a notable absence among the studied methods because of its high computational cost. Calculating the excess mass statistic has a high asymptotic complexity as the sample size n and the tested k grow. Despite approximations, the execution time under the recommended number of bootstrap samples ($B = 500$) was unworkable for reasonable values $n \geq 1000$ and $k > 1$. Moreover, the risks implied are magnified by the iterative use of the test, making it difficult to limit the total time per task. Therefore, we finally refrained from an exhaustive comparison. Nonetheless, preliminary experiments suggested a similar performance to FM in terms of accuracy.

Last but not least, the EIG method by Genovese et al. (2016), which we named after the role of the eigenvalues in its multivariate version, is based on very different principles, such as testing modes locally and splitting data into train and test sets. The confidence level for EIG was the same as in Genovese et al. (2016).

Software implementation. All the methods under study are coded in the R programming language. The source code for BTS, an R package, shall be distributed under licence and on demand. Our implementation relies on the package *robCompositions* for compositional data analysis (Templ et al., 2009). Our package will also include the source code for EIG by Genovese et al. (2016) and the data from the case study.

The rest of the methods are publicly available. GM is based on the classical package *mclust* (Scrucca et al., 1999, 2016). TS is implemented in *ftnonpar* (Davies and Kovac, 2012). The test-based approaches are provided in the package *multimode* by Ameijeiras-Alonso et al. (2021a) (see also Ameijeiras-Alonso et al., 2021b). Except for STE, which corresponds to the default routine `bw.SJ` in R with `method = "ste"`, all the bandwidth selectors are in the package *ks* (Duong, 2022).

D.2. Test-beds. The test-bed pdfs in Section 5.1 condense many different shapes, as seen in Fig. 13. In particular, Fig. 13e coincides with the example pdf in Fig. 2a. The five pdfs take the form $x \mapsto \sum_{i=1}^K w_i \phi((x - \mu_i)/\sigma_i)$, where ϕ is the standard Gaussian pdf, K is the number of mixture components and μ_i , σ_i and w_i are, respectively, the mean, the standard deviation and the weight of the i -th mixture component. Collecting all the mixture model parameters in vectors $\boldsymbol{\mu} = (\mu_1, \dots, \mu_K)$, $\boldsymbol{\sigma}^2 = (\sigma_1^2, \dots, \sigma_K^2)$ and $\boldsymbol{w} = (w_1, \dots, w_K)$, the five mixtures are defined in Table 3.

D.3. Rankings. The global and intermediate rankings in Table 1 and Table 2, respectively, are computed with the assistance of the R package *ConsRank* (D'Ambrosio

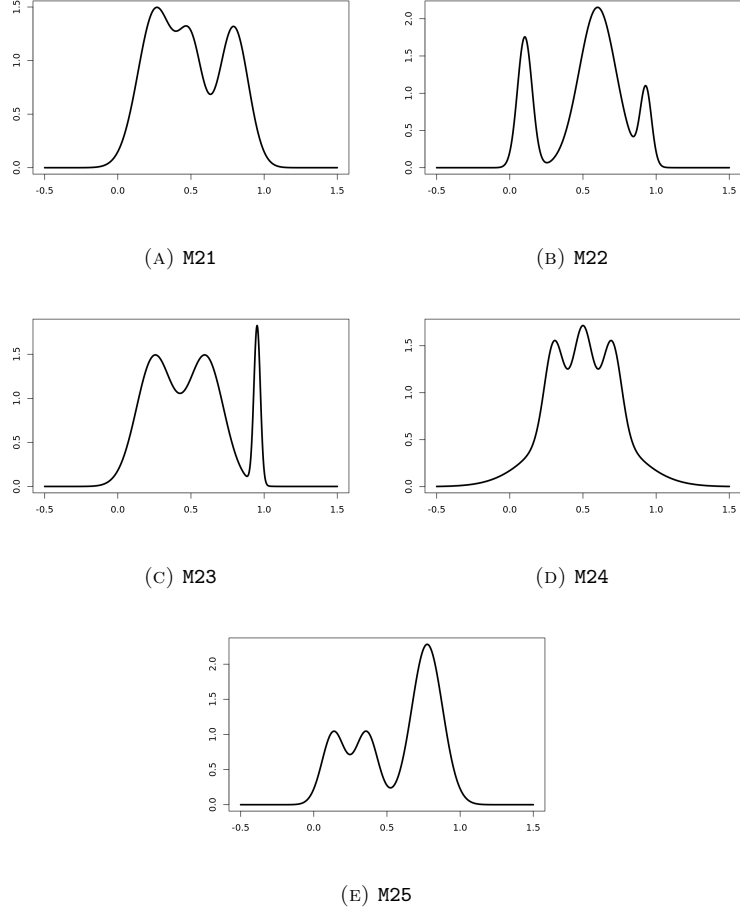


FIG. 13. Test-bed Gaussian mixture model pdfs.

	μ	σ^2	w
M21	(0.26, 0.79145, 0.5)	(0.01476, 0.01, 0.007)	(0.45, 0.33, 0.22)
M22	(0.6, 0.10245, 0.93)	(0.01588, 0.0025, 0.0015)	(0.68, 0.22, 0.1)
M23	(0.25, 0.6, 0.95222)	(0.015, 0.015, 0.00049)	(0.45, 0.45, 0.1)
M24	(0.5, 0.3, 0.5, 0.7)	(0.08425, 0.004, 0.004, 0.004)	(0.55, 0.15, 0.15, 0.15)
M25	(0.7749, 0.1345, 0.36)	(0.011, 0.006, 0.006)	(0.6, 0.2, 0.2)

TABLE 3. Test-bed Gaussian mixture model parameters.

et al., 2015). Namely, we used the routine `consrank` with all the default parameters except one for suppressing screen output. In particular, we selected `algorithm = "BB"`, corresponding to the *branch-and-bound* algorithm (Amodio et al., 2016), and `full = FALSE`, meaning ties were allowed among ranks.

APPENDIX E. EXTRA RESULTS

This section is a follow-up of the simulation study in Section 5.2 of the manuscript, including further results and comments.

E.1. Intermediate rankings. The rankings $\mathcal{R}_1, \dots, \mathcal{R}_{T \times S}$ in Table 2 are depicted in Fig. 14. The Kendall correlations between ranks are presented in Fig. 15. With

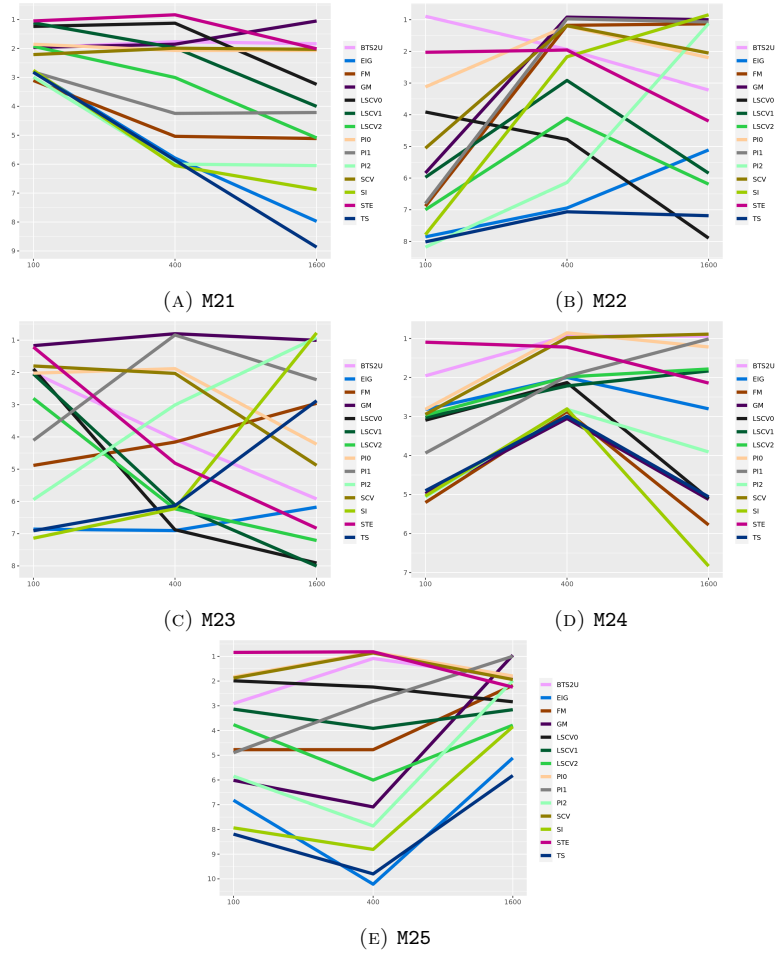


FIG. 14. Intermediate rankings in Table 2 by test-bed. In every subfigure, the horizontal and vertical axes correspond to the sample size and the rank of the method, respectively. A small amount of jitter has been added to the ranks to appreciate overlapping trajectories better.

these auxiliary representations, let us further analyse the results in Section 5.2 focusing on the less successful methods.

The two second-ranked methods apart from PI1, i.e., LSCV0 and LSCV1, also have some success. Contrary to PI1, the LSCV methods tend to under-smooth, helping to detect the short-lived mode in Fig. 13a. However, under-smoothing is counter-productive most of the time, leading to spurious modes as n grows. The last LSCV member, the third-ranked LSCV2, underperforms across all settings, securing zero first ranks.

The fifth-ranked PI2 goes deeper into regularisation than PI1, becoming too insensitive for most cases (see Fig. 14a, Fig. 14d and Fig. 14e). There are two first ranks in M22 and M23, though, always with $n = 1600$. Especially in M22, all the modes are long-lived and well-separated. Hence, the risk of not detecting them is outweighed by that of making up spurious ones. The fourth-placed method, FM, also shows top performance in M22-400 and M22-1600 for the same reason.

Among the sixth-ranked methods, we still see a top performance by SI in M22-1600 and M23-1600. Even though SI and FM appear highly correlated in Fig. 15, the former is dominated by the latter across most configurations. Nonetheless, both

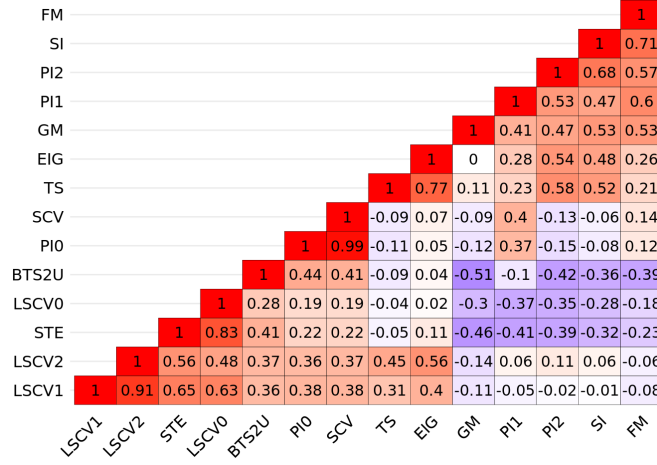


FIG. 15. Kendall correlations between the intermediate ranks in Table 2.

are *niche* methods that excel in some straightforward cases, with large sample sizes and well-separated modes. The same cannot be said about TS and EIG, which have no first positions and usually close the ranking, as depicted in Fig. 14a, Fig. 14b and Fig. 14e.

Table 2 also reveals noticeable differences among the first-ranked methods. GM negatively correlates with the other four, which are positively correlated among themselves. For instance, GM stands out with M23 while the rest struggle (see Fig. 14c) and the opposite happens with M24. On the other hand, PI0 and SCV usually perform best with medium to large sample sizes (see Fig. 14b), whereas STE operates better with small to medium ones (see Fig. 14a). The three KDEs are more or less even in the middle (Fig. 14d and Fig. 14e). The performance of BTS2U is mainly correlated with that of PI0 and, to a lesser extent, SCV and STE.

Some curiosities are found in Table 2. BTS2U is one of only three methods, alongside GM and STE, with an unmatched first rank, the M22-100 mentioned in the manuscript. Additionally, BTS2U is the only method not named GM capable of sustaining the first rank at least once in each of the three sample sizes. On the other hand, no method ranks first at least once in each of the five test-beds. The most versatile methods in that sense are GM, STE and PI1, with four.

E.2. Distribution. We will now look at the distribution of the predicted NoM in each of the $T \times S = 15$ sampling configurations through Fig. 16, Fig. 17, Fig. 18, Fig. 19, and Fig. 20. Here, the reader will see the *raw* accuracies and variabilities of each method in each scenario. We shall concentrate our commentary on some selected cases as the conclusions for the rest are qualitatively very similar.

Fig. 17a shows the top performance mentioned above for BTS2U, with a small sample size. BTS2U passes STE based on the significance of the results. The broad middle block of M22 traps STE and LSCV0 in over-predicting four modes. Meanwhile, GM misses the mode to the right many times. In turn, PI1, FM and EIG behave even more conservatively, while SI and PI2 get stuck at one and two modes, respectively. Interestingly, FM extends beyond three modes more than BTS2U.

A more complicated scenario is in Fig. 19c despite the large sample size. The model M24 is like the classic *claw* density used by Davies and Kovac (2004) but with three short-lived *fingers* instead of five. TS performs very well with the *claw* but not with M24, almost exclusively predicting one mode, similar to FM. Overall,

BTS0	BTS1S	BTS1J	BTS1U	BTS2S	BTS2J	BTS2U
2	1	1	1	1	1	1

TABLE 4. Global ranking among BTS variants.

M24 produces high variability, and almost all the methods widely spread their predictions over the one to five range. Having a lower accuracy, BTS2U ranks first, tied with three methods (PI0, PI1 and SCV) based on statistical significance. Very surprisingly, EIG manages to rank third ahead of GM and LSCV0. The latter is *off the chart*, as most of its predictions are above five. Lastly, SI lies at the bottom, predicting one mode 100% of the time.

The variability in Fig. 20b is the lowest of all the three cases considered. On the one hand, M22 is less complex than M25, but data is more scarce in Fig. 17a. On the other, M24 surpasses the complexity of M25, but with larger samples in Fig. 19c. In this case, BTS2U, PI0, SCV and STE rank at first, having very similar profiles between two and four modes. Only the three LSCV methods have predictions over four, while SI, TS and EIG are the only ones betting on one mode. Finally, FM surprisingly outperforms GM, which is excessively conservative.

The previous figures suggest many relevant correlations between the contending methods, as depicted in Fig. 21. We see several groups. BTS2U is similar to PI0, SCV and STE, while all the LSCV variants are highly concordant. A third group, loosely coupled, gathers TS, SI, GM, PI1, PI2 and FM, although PI1 also correlates with PI0. The fourth and final group comprises the outlying EIG, the only method with all its correlations below 0.5.

E.3. BTS variants. In Section 5.1, we chose BTS2U as our reference BTS variant to compare with the alternative traditional methods. Here, we will compare all the BTS variants in a similar exercise.

Table 4 shows the global ranking for the BTS variants. BTS0 ranks behind the rest, including BTS2U. The intermediate rankings are reported in Table 5 and depicted in Fig. 22. The rank correlations appear in Fig. 23.

The problem with BTS0 is the sample size: with large samples, it improves considerably, just like PI0 and PI1. On the other hand, the refined versions BTS2S, BTS2J and BTS2U are not significantly better than their respective predecessors, BTS1S, BTS1J and BTS1U.

Fig. 24 shows the correlations between the predictions of the methods. The refined versions are highly correlated with their respective base methods. In turn, we observe that the more biased the prior probabilities $\Pr(k)$ are, the higher the correlation with BTS0.

APPENDIX F. DIMENSIONALITY REDUCTION

This appendix expands on the dimensionality reduction in the analysis phase of BTS. First, we outline the technicalities of SFPCA. Then, we address the requests of two reviewers for further justification on picking just the first PC.

F.1. SFPCA. The following lines discuss SFPCA in our context for $\mathcal{Z}_d[a, b]$. We translate the original theory in Hron et al. (2016) to our notation so the reader can more easily identify the elements involved.

Let us express the CLR of each of the d PCs in terms of ZB-spline basis functions as $\text{clr}[PC_i] = \sum_{j=1}^d \mathbf{b}_i^j Z_j$. That is, each PC_i corresponds to the column vector $\mathbf{b}_i = (\mathbf{b}_i^1, \dots, \mathbf{b}_i^d) \in \mathbb{R}^d$. Similarly, let us also expand the centred functional data

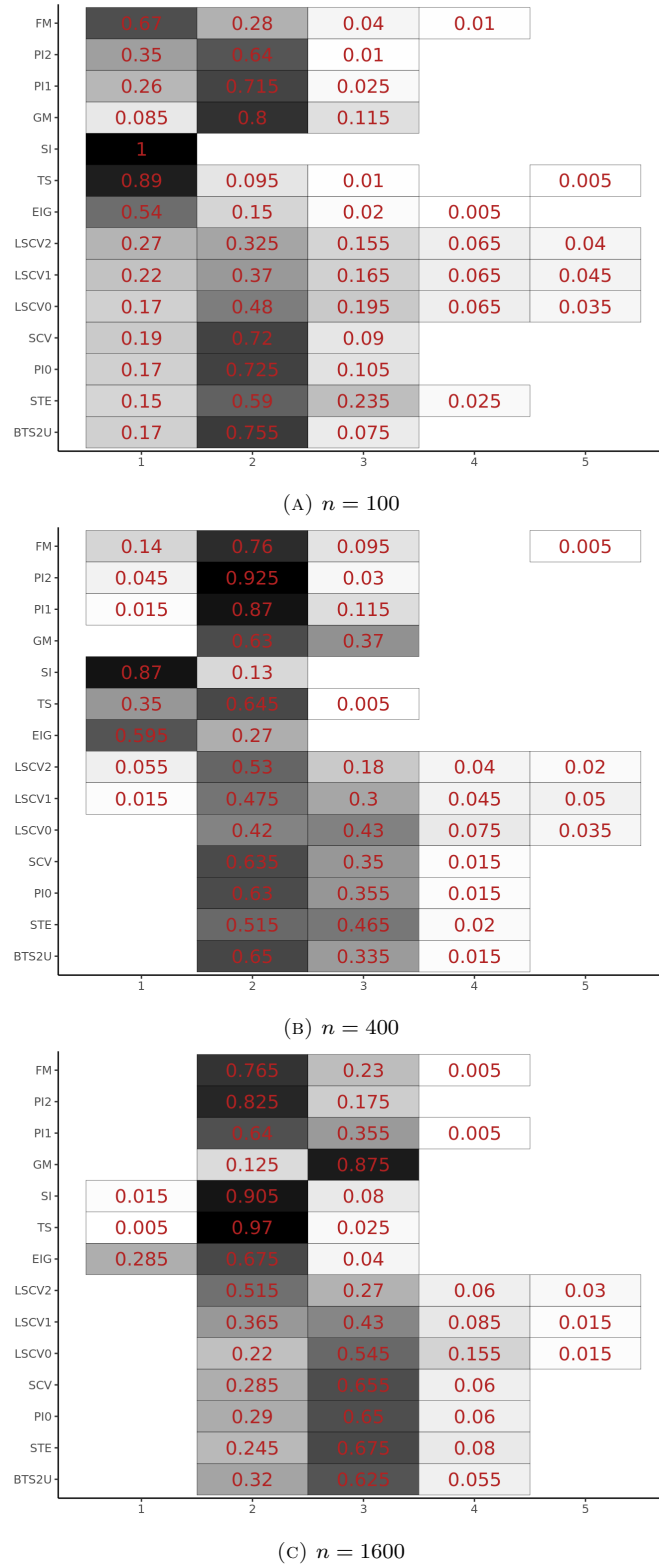
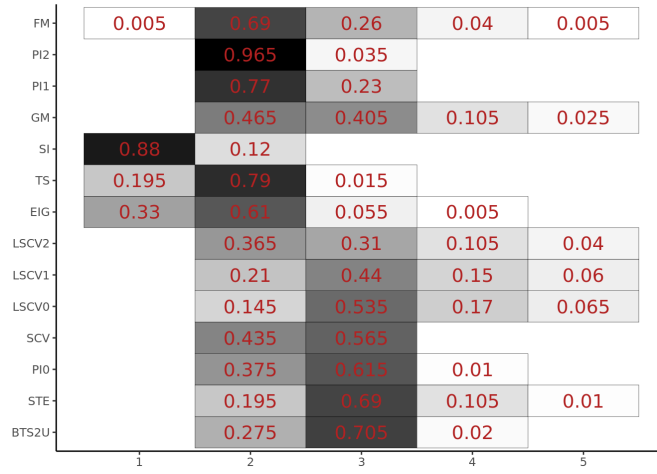
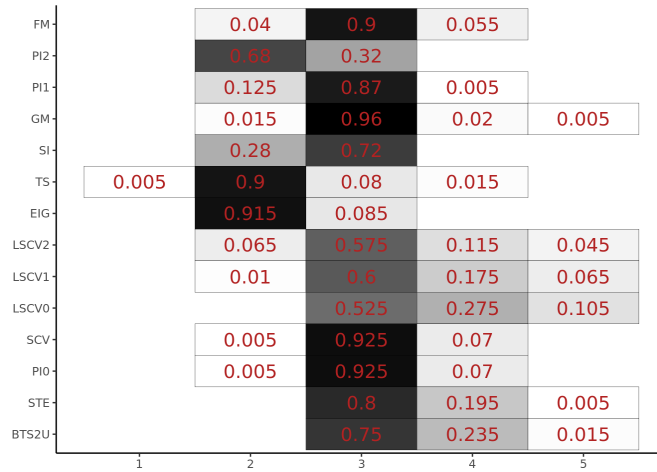


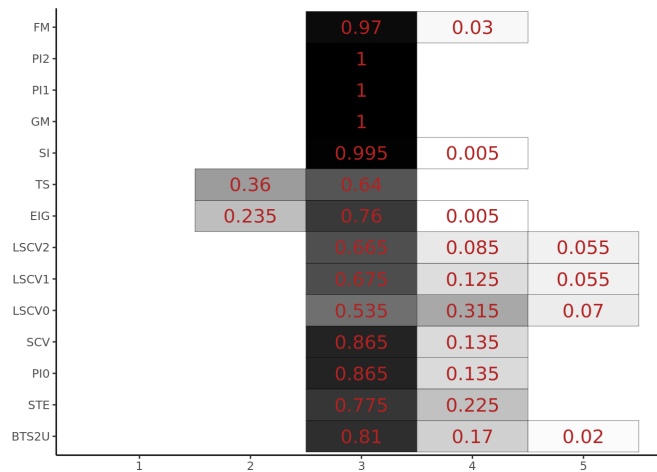
FIG. 16. Distribution of the predicted NoM for the M21 test-bed for several sample sizes n .



(A) $n = 100$

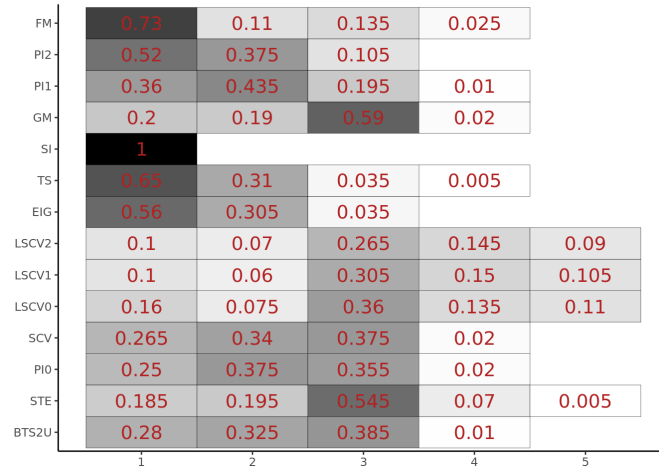


(B) $n = 400$

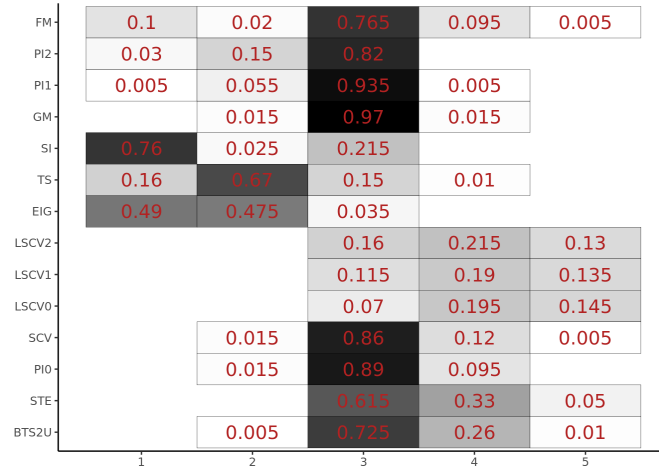


(C) $n = 1600$

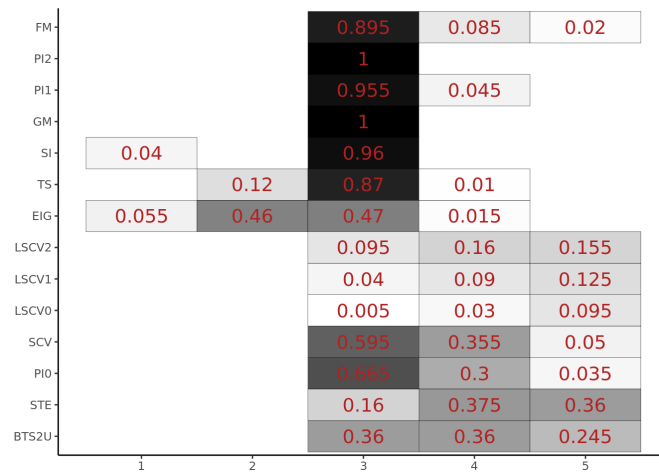
FIG. 17. Distribution of the predicted NoM for the M22 test-bed for several sample sizes n .



(A) $n = 100$



(B) $n = 400$



(C) $n = 1600$

FIG. 18. Distribution of the predicted NoM for the M23 test-bed for several sample sizes n .

FM	0.955	0.03	0.01	0.005	
PI2	0.735	0.245	0.02		
PI1	0.855	0.285	0.05	0.01	
GM	0.935	0.065			
SI	1				
TS	0.995	0.005			
EIG	0.335	0.425	0.11	0.005	
LSCV2	0.42	0.155	0.06	0.06	0.08
LSCV1	0.44	0.11	0.08	0.08	0.075
LSCV0	0.465	0.17	0.09	0.075	0.09
SCV	0.505	0.345	0.11	0.04	
PI0	0.46	0.36	0.13	0.05	
STE	0.435	0.275	0.17	0.085	0.03
BTS2U	0.46	0.315	0.17	0.05	0.005
	1	2	3	4	5

(A) $n = 100$

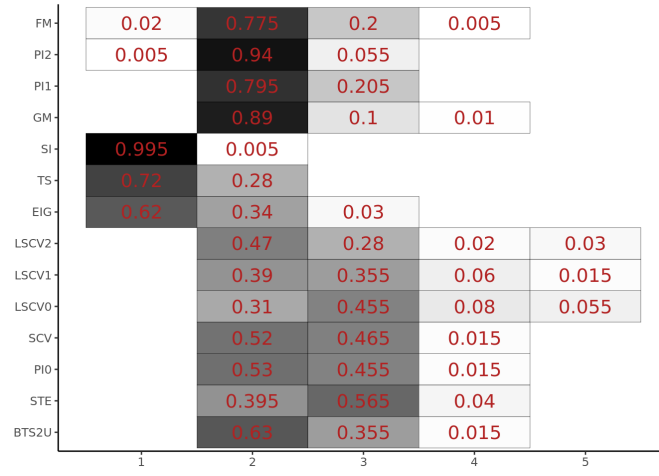
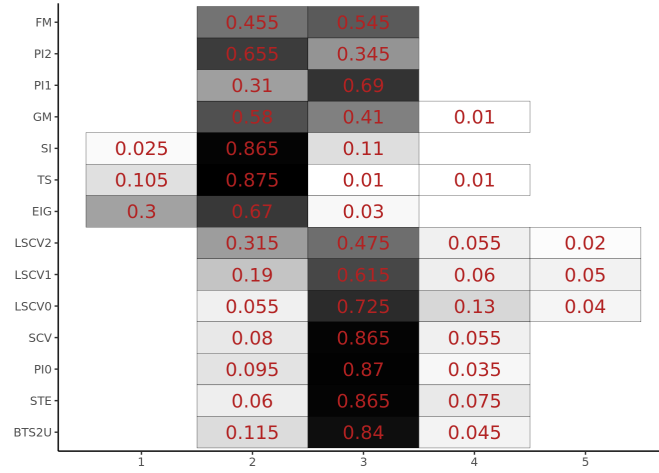
FM	0.935	0.06		0.005	
PI2	0.77	0.21	0.015	0.005	
PI1	0.54	0.34	0.095	0.015	0.005
GM	0.965	0.03	0.005		
SI	1				
TS	0.99	0.01			
EIG	0.4	0.305	0.085	0.01	
LSCV2	0.175	0.11	0.145	0.105	0.09
LSCV1	0.14	0.08	0.14	0.16	0.125
LSCV0	0.07	0.115	0.1	0.145	0.185
SCV	0.205	0.31	0.33	0.11	0.035
PI0	0.195	0.3	0.345	0.105	0.045
STE	0.165	0.22	0.275	0.17	0.12
BTS2U	0.265	0.29	0.3	0.085	0.05
	1	2	3	4	5

(B) $n = 400$

FM	0.885	0.055	0.03	0.02	
PI2	0.605	0.29	0.095	0.01	
PI1	0.2	0.29	0.335	0.13	0.04
GM	0.305	0.63	0.055	0.01	
SI	1				
TS	0.835	0.12	0.045		
EIG	0.39	0.345	0.12	0.015	
LSCV2	0.03	0.08	0.205	0.19	0.11
LSCV1	0.01	0.04	0.13	0.2	0.135
LSCV0			0.055	0.115	0.18
SCV	0.02	0.07	0.325	0.3	0.205
PI0	0.02	0.075	0.325	0.3	0.215
STE	0.005	0.025	0.16	0.295	0.265
BTS2U	0.19	0.14	0.235	0.245	0.125
	1	2	3	4	5

(C) $n = 1600$

FIG. 19. Distribution of the predicted NoM for the M24 test-bed for several sample sizes n .

(A) $n = 100$ (B) $n = 400$ (C) $n = 1600$ FIG. 20. Distribution of the predicted NoM for the M25 test-bed for several sample sizes n .

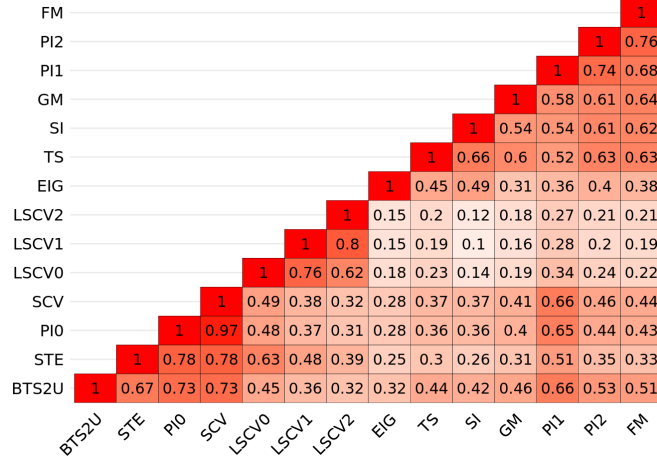


FIG. 21. Kendall correlations between predictions along the $T \times S \times m = 3000$ samples.

	BTS0	BTS1S	BTS1J	BTS1U	BTS2S	BTS2J	BTS2U
M21	100	2	2	1	1	2	1
M21	400	3	2	2	1	2	2
M21	1600	3	2	2	1	2	2
M22	100	3	2	2	1	2	2
M22	400	1	2	2	3	2	2
M22	1600	1	2	2	3	2	2
M23	100	4	3	2	1	3	2
M23	400	1	2	2	3	2	2
M23	1600	1	2	2	2	2	2
M24	100	2	2	1	1	2	1
M24	400	4	3	2	1	3	2
M24	1600	1	1	1	1	1	1
M25	100	4	3	2	1	3	2
M25	400	2	1	1	1	1	1
M25	1600	1	2	2	2	2	2

TABLE 5. Intermediate rankings by test-bed and sample size configuration among BTS variants.

as $\text{clr}[\zeta_{\theta_i} \ominus \mu] = \sum_{j=1}^d \mathbf{C}_{ij} Z_j$, i.e., the coordinates forming the rows of the matrix $\mathbf{C} \in \mathbb{R}^{\nu \times d}$.

To obtain \mathbf{b}_i , we *first* have to solve the i -th largest eigenvalue λ_i problem

$$\frac{1}{\nu} \mathbf{M}^{1/2} \mathbf{C}^\top \mathbf{C} \mathbf{M}^{1/2} \mathbf{u}_i = \lambda_i \mathbf{u}_i, \quad (\text{S1})$$

where $\mathbf{u}_i \in \mathbb{R}^d$ has Euclidean norm one, i.e., $\mathbf{u}_i^\top \mathbf{u}_i = 1$, and $\mathbf{M}^{1/2}$ is the square root of the ZB-spline inner product matrix \mathbf{M} defined in Section 2. Problem (S1) corresponds to the usual principal component analysis in \mathbb{R}^d for the transformed data matrix $\mathbf{C} \mathbf{M}^{1/2}$ (Hron et al., 2016, p. 5) and can be solved directly using the routine `eigen` in R. Then, finally, one takes \mathbf{b}_i satisfying $\mathbf{M}^{1/2} \mathbf{b}_i = \mathbf{u}_i$, while the corresponding eigenvalue is λ_i .

Considering the solutions of all the λ_i -problems (S1), it can be easily checked that $\langle \text{PC}_i, \text{PC}_j \rangle_{\mathcal{B}} = \mathbf{b}_i^\top \mathbf{M} \mathbf{b}_j = \mathbf{u}_i^\top \mathbf{u}_j = \delta_{ij}$, the Kronecker delta, meaning the

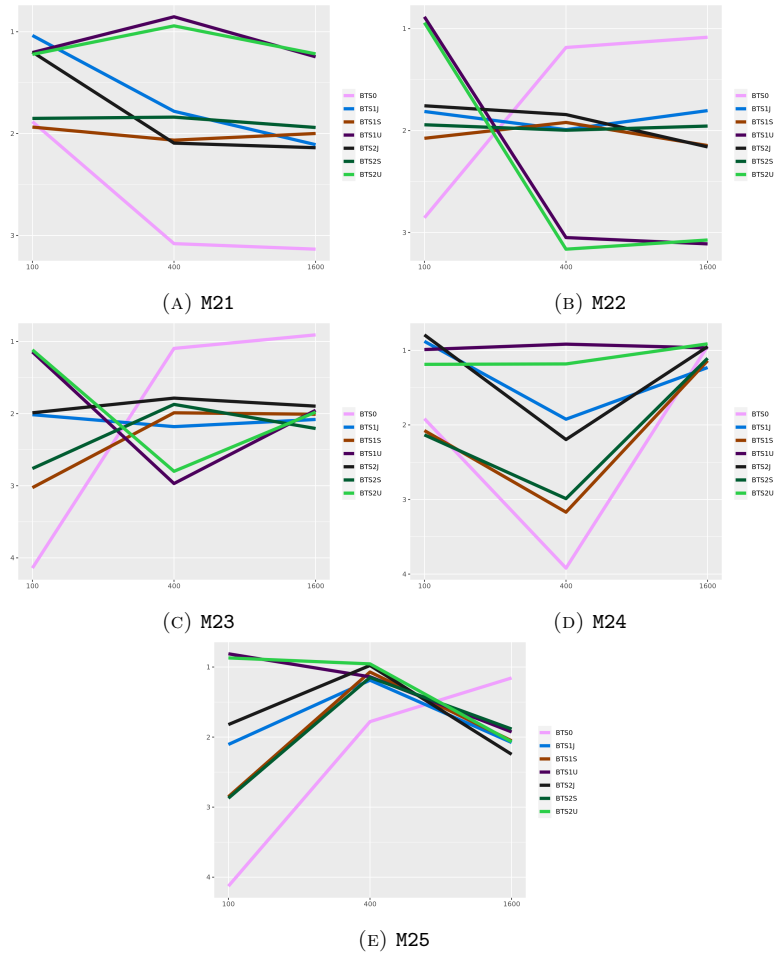


FIG. 22. Intermediate rankings by test-bed among BTS variants.

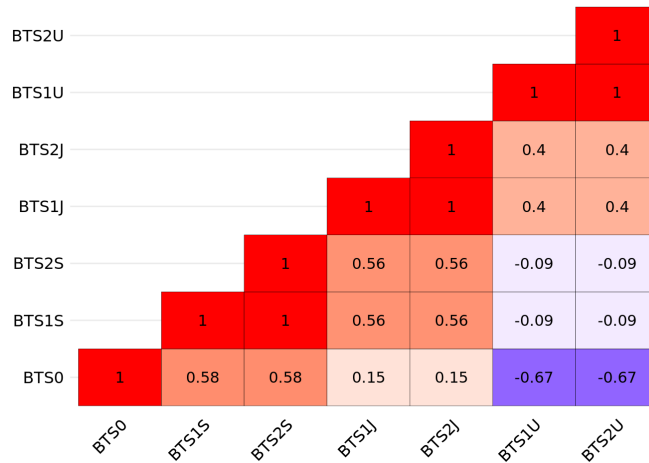


FIG. 23. Kendall correlations between the intermediate ranks in Table 5.



FIG. 24. Kendall correlations between predictions for the NoM along the $T \times S \times m = 3000$ samples for the BTS variants.

PCs form an orthonormal basis. To grasp the true meaning of PCs, specifically their variability-maximising property, we refer the reader to Hron et al. (2016). In particular, the sum of squared scores $\sum_{i=1}^{\nu} s_i^2$ (see Section 3.2) is maximal when a unitary PC_1 is the first PC (Hron et al., 2016, Equation 7).

F.2. Dimension justification. In Section 3.2 of the manuscript, we sketched some convenience and simplicity reasons behind keeping just one dimension coincidental with the goals of the analysis phase. Namely, we alluded to making robust inferences and improving interpretability. We also claimed that one PC provided enough power in the BTS context but gave no justification beyond the scree plot in Fig. 4a, complemented in this SM with Fig. 11a. Let us now imagine the consequences of including several PCs.

First, the multiparameter generalisation of (9) is

$$\Pr(\cdot | \delta_1, \dots, \delta_\ell) = \mu \oplus \bigoplus_{i=1}^{\ell} (\delta_i \odot \sigma_i), \quad (\text{S2})$$

where μ stays the same as in (9), $\sigma_i = \sqrt{\lambda_i} \odot PC_i$, and typically $\ell \ll d$. A similar procedure based on centred projections allows prescribing a rectangular support for the parameter vector $(\delta_1, \dots, \delta_\ell)$.

Using (S2), new information would enter into our analysis. Though valuable for other purposes, such information would be noisy and redundant for estimating the NoM. By *debugging* samples like that in Fig. 3, we observed that many different but similar pdfs lead to the same NoM. The second and subsequent PCs generally add variability regarding other pdf properties. For instance, in some scenarios, mode A is higher than mode B, while in others, it is the other way around. Similarly, modes A and B appear in slightly different positions in some scenarios. Taking all into account, we would end up with a complex model like (S2), where several δ_i have to be tuned, increasing the computational cost and reducing the robustness of the inference process. Moreover, making sense of such an analysis would be challenging compared to the simplicity of Fig. 6a. In particular, note that the mode tree in Fig. 6a does not say anything about the height of a mode.

The above explanation about redundancy and noise will be more apparent after examining the modes of variation for the subsequent PCs in Fig. 25. First, note that the amplitude of the *oscillations* around the mean gets increasingly weak from

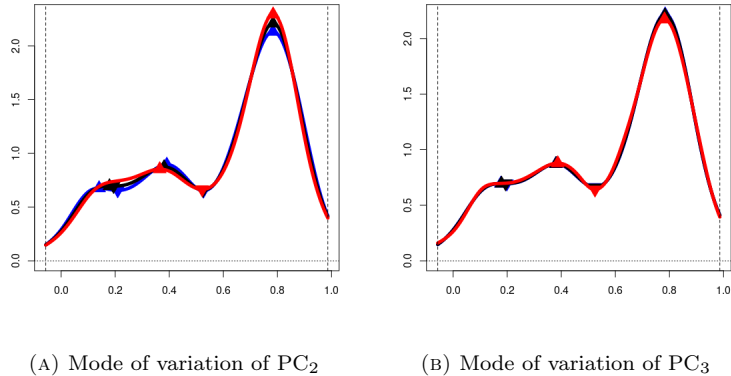


FIG. 25. Modes of variation for subsequent PCs following the example in Fig. 4. Both subfigures have the same structure and colouring conventions as Fig. 4b, but replacing PC₁ with PC₂ and PC₃, respectively. Also, the black curve in both cases is the same as in Fig. 4b, corresponding to the mean μ . The support bounds δ_{\min} and δ_{\max} are calculated analogously as for (10), considering PC₂ or PC₃ instead of PC₁. On the left, the lower bound (blue) has three modes, while the upper bound (red) has two. By contrast, the situation in the right-hand side subfigure is unclear, given the small amplitude of the *oscillation* around the mean.

Fig. 4b to Fig. 25a and then Fig. 25b. In fact, the *oscillation* for PC₃ is already virtually imperceptible in Fig. 25b, being PC₃ arguably noisy. The case of Fig. 25a is far more interesting, however. There, we see that the pdf in which the two left-most modes are most pronounced (the blue curve) is also the one in which the right-most mode has the lowest height. That is precisely the opposite case of Fig. 4b, where the three modes grow simultaneously. This means that PC₂ is associated with calibrating the relative height of the modes, which is redundant for estimating the NoM.

There is a natural reason why one PC works so well. One has to consider that the set of functions $\{\zeta_{\theta_i}\}_{i=1}^{\nu}$ we aim to summarise with SFPCA has a relatively low complexity compared to arbitrary datasets in functional data analysis. The random mechanism generating them is comparatively straightforward: a joint use of KDE and compositional splines. The complementary interaction between h and α in Fig. 3 should be relatively simple to capture with a single PC. In this respect, we note that an oblique straight boundary, like in Fig. 3, is standard but not universal, as shown in Fig. 10. In the latter case, the boundary is vertical, indicating an even simpler scenario dominated by h .

Finally, adding more PCs would also be inconvenient for two reasons. First, we would no longer be able to pick a median spline representative \tilde{f}_k of each k -modality hypothesis for the testing phase, at least not directly and efficiently, as in the one-dimensional case. Also, the Jeffreys prior in (10) in the one-dimensional case has the desirable property of being a *reference prior*, which does not happen in the multiparameter setting (Bernardo, 1994).

APPENDIX G. COMPUTING

This section comments on the computational environment used throughout our investigation. Emerging technologies such as *containerisation* and *cloud computing*

are increasingly drawing the attention of the research community as a means to enhance reproducibility.

Containerisation. All our research outputs have been produced within a *Docker* container (Merkel, 2014). The figures and tables were generated upon building a Docker image as part of the installed vignettes of an R package. The *Dockerfile* with the specification of that image will be distributed along the BTS package for R. Next, the built image was made available for the simulation study in a private *cloud* environment through the *Docker Hub* container registry.

Cloud computing. The simulation study was carried out with the help of Microsoft’s *Azure Databricks* service (Etaati, 2019). The whole experiment was scheduled as a Databricks *workflow*, where each of the $T \times S = 15$ sampling configurations was a Databricks *task* executing a Databricks R *notebook* with distinct parameters. Then, the $m = 200$ replications took the form of parallelisable Spark *tasks* (Karau and Warren, 2017). The required R files and a JSON file specifying the workflow will be distributed along the BTS package. Finally, the workflow job was assigned to a Databricks cluster with 25 type *Standard_DS3_v2* workers, each counting on four cores. Therefore, 100 threads ran in parallel at any given time for a total execution time of approximately 20 hours.

REFERENCES

- AMELJEIRAS-ALONSO, J. (2017). “Assessing simplifying hypotheses in density estimation”. PhD thesis. Universidade de Santiago de Compostela.
- AMELJEIRAS-ALONSO, J., CRUJEIRAS, R. M., and RODRÍGUEZ-CASAL, A. (2018). Mode testing, critical bandwidth and excess mass. *TEST* **28**, 900–19.
- AMELJEIRAS-ALONSO, J., CRUJEIRAS, R. M., and RODRÍGUEZ-CASAL, A. (2021b). Multimode: an R package for mode assessment. *Journal of Statistical Software* **97**.
- AMODIO, S., D’AMBROSIO, A., and SICILIANO, R. (2016). Accurate algorithms for identifying the median ranking when dealing with weak and partial rankings under the Kemeny axiomatic approach. *European Journal of Operational Research* **249**, 667–76.
- BERNARDO, J. M. (1994). Bayesian statistics. *Probability and statistics*. Vol. 2, 345–407.
- BOOR, C. DE (1972). On calculating with B-splines. *Journal of Approximation Theory* **6**, 50–62.
- CHACÓN, J. E. and DUONG, T. (2013). Data-driven density derivative estimation, with applications to nonparametric clustering and bump hunting. *Electronic Journal of Statistics* **7**, 499–532.
- CHACÓN, J. E. and DUONG, T. (2018). *Multivariate kernel smoothing and its applications*. Chapman and Hall/CRC.
- CHAUDHURI, P. and MARRON, J. S. (1999). SiZer for exploration of structures in curves. *Journal of the American Statistical Association* **94**, 807–23.
- CHAUDHURI, P. and MARRON, J. S. (2002). Curvature vs. slope inference for features in nonparametric curve estimates. *Unpublished manuscript*.
- DAVIES, L., GATHER, U., NORDMAN, D., and WEINERT, H. (2009). A comparison of automatic histogram constructions. *ESAIM: Probability and Statistics* **13**, 181–96.
- DAVIES, L. and KOVAC, A. (2004). Densities, spectral densities and modality. *The Annals of Statistics* **32**, 1093–136.
- DONOHO, D. L. (1988). One-sided inference about functionals of a density. *The Annals of Statistics* **16**, 1390–420.
- EILERS, P. H. C. and MARX, B. D. (1996). Flexible smoothing with B-splines and penalties. *Statistical Science* **11**, 89–121.
- ETAATI, L. (2019). “Azure Databricks”. *Machine learning with Microsoft technologies*. Apress, 159–71.
- GENOVESE, C., PERONE-PACIFICO, M., VERDINELLI, I., and WASSERMAN, L. (2016). Non-parametric inference for density modes. *Journal of the Royal Statistical Society: Series B (Statistical Methodology)* **78**, 99–126.
- GOOD, I. J. and GASKINS, R. A. (1980). Density estimation and bump-hunting by the penalized likelihood method exemplified by scattering and meteorite data. *Journal of the American Statistical Association* **75**, 42–56.
- GRAMACKI, A. and GRAMACKI, J. (2017). FFT-based fast bandwidth selector for multivariate kernel density estimation. *Computational Statistics & Data Analysis* **106**, 27–45.

- HRON, K., MENAFOGLIO, A., TEMPL, M., HRŮZOVÁ, K., and FILZMOSER, P. (2016). Simplicial principal component analysis for density functions in Bayes spaces. *Computational Statistics & Data Analysis* **94**, 330–50.
- KARAU, H. and WARREN, R. (2017). *High performance spark: best practices for scaling and optimizing Apache Spark*. O’Reilly Media, Incorporated.
- KASS, R. E. and RAFTERY, A. E. (1995). Bayes factors. *Journal of the American Statistical Association* **90**, 773–95.
- KLUGKIST, I., KATO, B., and HOIJTINK, H. (2005). Bayesian model selection using encompassing priors. *Statistica Neerlandica* **59**, 57–69.
- MACHALOVÁ, J., TALSKÁ, R., HRON, K., and GÁBA, A. (2020). Compositional splines for representation of density functions. *Computational Statistics* **36**, 1031–64.
- MERKEL, D. (2014). Docker: lightweight Linux containers for consistent development and deployment. *Linux J.* **2014**.
- MINNOTTE, M. C. (1997). Nonparametric testing of the existence of modes. *The Annals of Statistics* **25**, 1646–60.
- MINNOTTE, M. C., MARCHETTE, D. J., and WEGMAN, E. J. (1998). The bumpy road to the mode forest. *Journal of Computational and Graphical Statistics* **7**, 239–51.
- MINNOTTE, M. C. and SCOTT, D. W. (1993). The mode tree: a tool for visualization of nonparametric density features. *Journal of Computational and Graphical Statistics* **2**, 51–68.
- SCRUCCA, L., FOP, M., MURPHY, T. B., and RAFTERY, A. E. (2016). mclust 5: clustering, classification and density estimation using Gaussian finite mixture models. *The R Journal* **8**, 289–317.
- SPIEGELHALTER, D. J., BEST, N. G., CARLIN, B. P., and LINDE, A. VAN DER (2014). The deviance information criterion: 12 years on. *Journal of the Royal Statistical Society: Series B (Statistical Methodology)* **76**, 485–93.
- WAGENMAKERS, E.-J., LODEWYCKX, T., KURIYAL, H., and GRASMAN, R. (2010). Bayesian hypothesis testing for psychologists: a tutorial on the Savage–Dickey method. *Cognitive Psychology* **60**, 158–89.
- WAND, M. P. and JONES, M. C. (1995). *Kernel smoothing*. Springer US.
- WASSERMAN, L. (2000). Bayesian model selection and model averaging. *Journal of Mathematical Psychology* **44**, 92–107.

RESOURCES

- AMEIJEIRAS-ALONSO, J., CRUJEIRAS, R. M., and RODRÍGUEZ-CASAL, A. (2021a). *multimode. Mode testing and exploring*. Version 1.5. URL: <https://cran.r-project.org/package=multimode>.
- D’AMBROSIO, A., AMODIO, S., MAZZEO, G., ALBANO, A., and PLAIA, A. (2015). *ConsRank. Compute the median ranking(s) according to the Kemeny’s axiomatic approach*. Version 2.1.0. URL: <https://cran.r-project.org/package=ConsRank>.
- DAVIES, L. and KOVAC, A. (2012). *ftnonpar. Features and strings for nonparametric regression*. Version 0.1-88. URL: <https://cran.r-project.org/package=ftnonpar>.
- DUONG, T. (2022). *ks. Kernel smoothing*. Version 1.13.5. URL: <https://cran.r-project.org/package=ks>.
- PETTI, B. and GILANI, S. (2022). *baseballr. Acquiring and analyzing baseball data*. Version 1.5.0. URL: <https://cran.r-project.org/web/packages/baseballr/index.html>.
- SCRUCCA, L., FOP, M., MURPHY, T. B., and RAFTERY, A. E. (1999). *mclust. Gaussian mixture modelling for model-based clustering, classification, and density estimation*. URL: <https://cran.r-project.org/package=mclust>.
- TEMPL, M., HRON, K., and FILZMOSER, P. (2009). *robCompositions. Compositional data analysis*. Version 2.3.1. URL: <https://cran.r-project.org/package=robCompositions>.
- WILLMAN, D. (2023). *BaseballSavant*. URL: <https://baseballsavant.mlb.com/>.

Authors: JOSÉ E. CHACÓN[†] AND JAVIER FERNÁNDEZ SERRANO[‡].

[†]DEPARTAMENTO DE MATEMÁTICAS, UNIVERSIDAD DE EXTREMADURA, BADAJOZ, SPAIN.

[‡]DEPARTAMENTO DE MATEMÁTICAS, UNIVERSIDAD AUTÓNOMA DE MADRID, MADRID, SPAIN.

E-mail addresses: [†]jechacon@unex.es ✉, [‡]javier.fernandezs01@estudiante.uam.es.

[†]<https://orcid.org/0000-0002-3675-1960> .

[‡]<https://orcid.org/0000-0001-5270-9941> .